© 2021. Published by The Company of Biologists Ltd | Development (2021) 148, dev195875. doi:10.1242/dev.195875

RESEARCH ARTICLE

The intrinsically disordered protein SPE-18 promotes localized assembly of MSP in *Caenorhabditis elegans* spermatocytes

Kari L. Price*,¶, Marc Presler‡,¶, Christopher M. Uyehara§ and Diane C. Shakes

ABSTRACT

Many specialized cells use unconventional strategies of cytoskeletal control. Nematode spermatocytes discard their actin and tubulin following meiosis, and instead employ the regulated assembly/disassembly of the Major Sperm Protein (MSP) to drive sperm motility. However, prior to the meiotic divisions, MSP is sequestered through its assembly into paracrystalline structures called fibrous bodies (FBs). The accessory proteins that direct this sequestration process have remained mysterious. This study reveals SPE-18 as an intrinsically disordered protein that is essential for MSP assembly within FBs. In *spe-18* mutant spermatocytes, MSP forms disorganized cortical fibers, and the cells arrest in meiosis without forming haploid sperm. In wild-type spermatocytes, SPE-18 localizes to pre-FB complexes and functions with the kinase SPE-6 to localize MSP assembly. Changing patterns of SPE-18 localization uncover previously unappreciated complexities in FB maturation. Later, within newly individualized spermatids, SPE-18 is rapidly lost, yet SPE-18 loss alone is insufficient for MSP disassembly. Our findings reveal an alternative strategy for sequestering cytoskeletal elements, not as monomers but in localized, bundled polymers. Additionally, these studies provide an important example of disordered proteins promoting ordered cellular structures.

KEY WORDS: Major sperm protein, Intrinsically disordered protein, *Caenorhabditis elegans*, Spermatogenesis, Cytoskeletal assembly, *spe-18*

INTRODUCTION

The ability of cells to move, divide, and assume specific cell shapes requires a cytoskeleton that can reversibly assemble into a wide range of structures. Core to this flexibility is the intrinsic capacity of core molecular subunits to polymerize into filaments. The subsequent process of regulating how, when and where these filaments assemble into larger molecular superstructures is directed by a wide diversity of modifier and accessory proteins (Hohmann and Dehghani, 2019; Rottner et al., 2017; Goodson and Jonasson, 2018). Current concepts of cytoskeletal regulation have been dominated by functional studies of actin and tubulin and their interactions with diverse accessory proteins (Svitkina, 2018; Buracco et al., 2019; Brouhard and Rice, 2018; Bodakuntla et al., 2019; de Forges et al., 2012). However, a full understanding of cytoskeletal control requires consideration of less-studied proteins whose properties challenge our standard assumptions.

One such protein is the nematode Major Sperm Protein (MSP), assembly/disassembly dynamics of which power the crawling motility of nematode spermatozoa (Klass and Hirsh, 1981; Sepsenwol et al., 1989; Italiano et al., 1996; reviewed by Roberts and Stewart, 2012; Smith, 2014). Although MSP-based motility appears superficially similar to its actin-based counterpart, the molecular mechanisms are distinct. Much of what we know about MSP dynamics was gleaned from the parasitic nematode *Ascaris*, whose sperm size and number makes *Ascaris* sperm amenable for biochemical analyses. MSP lacks nucleotide binding sites and is quite small, only 14 kDa (Roberts, 2005). Importantly, whereas polarity is a hallmark of actin and tubulin assembly, MSP monomers form symmetric homodimers that subsequently form apolar filaments (Bullock et al., 1998). Because MSP filaments lack polarity, they are not associated with molecular motors, and their unidirectional growth requires accessory proteins. *In vitro* comet assays show that the integral membrane protein MSP polymerization-organizing protein (MPOP) is sufficient for localized MSP polymerization (LeClaire et al., 2003). However, within crawling spermatozoa, the localized assembly of MSP filaments involves several additional factors including a serine/threonine (ser/thr) kinase MPAK; a filament assembly factor, MFP2, that is activated by MSP polymerization-activating kinase (MPAK); a growing end-capping protein, MFP1; and a filament-stabilizing factor, MFP3 (Roberts and Stewart, 2012). Disassembly of MSP filaments at the base of the pseudopod involve dephosphorylation of MFP3 by a PP2A phosphatase (Yi et al., 2009).

Non-flagellated, crawling spermatozoa are a defining feature of the phylum Nematoda, and these MSP-propelled cells are both remarkably speedy (Italiano et al., 1999) and highly efficient; in the hermaphroditic species *Caenorhabditis elegans*, every sperm successfully fertilizes an oocyte (Singson, 2001). Yet the developmental program required to produce these spermatozoa includes both assets and challenges. In *C. elegans*, where it has been best studied, spermatogenesis occurs in a linear developmental sequence along the length of the gonad (Fig. 1A). Instead of taking days to weeks as in *Drosophila* and vertebrates, progression through the stages of meiotic prophase takes less than 24 h (Jaramillo-Lambert et al., 2007; Fig. 1A,C,D), and post-meiotic development is abbreviated to minutes rather than days (Chu and Shakes, 2013; Hu et al., 2019). Two key factors account for the brevity of the post-meiotic process. First, instead of having to remodel actin and tubulin into specialized structures following the meiotic divisions, nematode spermatocytes discard actin and tubulin into a central residual body, and MSP takes over as the core cytoskeletal element (Nelson et al., 1982; Ward, 1986; Winter et al., 2017; Fig. 1E). Second, during meiotic prophase, nematode spermatocytes must synthesize and pre-package all of the components needed to support post-meiotic sperm

Department of Biology, William & Mary, Williamsburg, VA 23187, USA.
*Present address: Department of Genetics, Yale University School of Medicine, New Haven, CT 06511, USA. ‡Present address: Applied BioMath LLC, Concord, MA 01742, USA. §Present address: Department of Genetics, The University of North Carolina at Chapel Hill, Chapel Hill, NC 27599, USA.
¶These authors contributed equally to this work

**Author for correspondence (dcshak@wm.edu)

K.L.P., 0000-0001-6099-9686; M.P., 0000-0002-0182-8075; C.M.U., 0000-0002-3210-9428; D.C.S., 0000-0002-9677-5577

Handling Editor: Swathi Arur
Received 10 August 2020; Accepted 2 February 2021

Development (2021) 148, dev195875. doi:10.1242/dev.195875

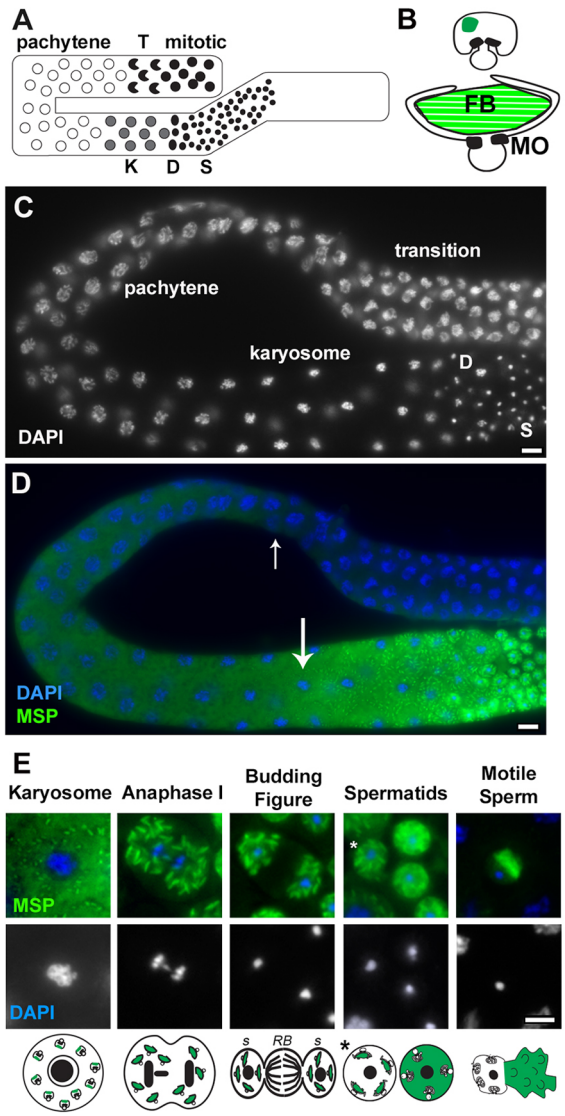

Fig. 1. Overview of *C. elegans* spermatogenesis. (A) Schematic of the adult male gonad highlighting its linear organization. After proliferating mitotically at the distal end, undifferentiated germ cells commit to spermatogenesis as they transition (T) to meiotic prophase and enter an extended pachytene stage. Towards the end of meiotic prophase, the spermatocytes enter the karyosome stage (K) during which the chromosomes compact and global transcription ceases. Following a narrow zone of meiotically dividing spermatocytes (D), quiescent haploid spermatids (S) accumulate in the seminal vesicle. (B) Schematics of early (top) and fully mature (bottom) Golgi-derived fibrous body-membranous organelle (FB-MO) complexes. FBs develop on the cytoplasmic surface of the MOs. Ultimately, the arms of the MO partially surround the MSP-enriched FB (green). An electron-dense collar separates this domain from the glycoprotein-filled MO vesicle. (C,D) Isolated male gonad showing stage-specific chromatin morphology by DAPI staining (C) and co-labeling with anti-MSP (green) to show initial expression in pachytene spermatocytes (small arrow) and distinct FBs (large arrow) in karyosome stage spermatocytes (D). (E) Stage-specific patterns of MSP distribution in spermatocytes and in schematics. During nematode spermatogenesis, anaphase II is followed by a partitioning, budding figure stage during which the cell's actin, microtubules and ribosomes are discarded in a central residual body (RB) as the FB-MO complexes, mitochondria and chromatin partition to the spermatids. Once spermatids detach from the RBs, all but the most recently individualized (asterisks) contain MOs that have docked but not fused with the plasma membrane and FBs that have disassembled to release MSP dimers throughout the cytoplasm. In activated, motile sperm, the MOs form stable fusion pores with the plasma membrane of the cell body, and MSP localizes to the pseudopod. Scale bars: 5 µm.

functions. Global transcription ceases near the end of meiotic prophase, precluding any post-meiotic burst of sperm-specific transcription (Shakes et al., 2009), and protein synthesis ceases as the cell's ribosomes are discarded into the residual body (Ward et al., 1981). These efficiencies are countered by the challenge of how to control the potentially disruptive random self-assembly of MSP, particularly as MSP levels reach 10-15% of the total and 40% of the soluble cellular protein (Roberts, 2005).

Developing spermatocytes address this challenge by assembling MSP into a distinct, stable and sequestered form (Fig. 1). Little is known about the accessory proteins that govern this alternate mode of MSP assembly. However, imaging in *C. elegans* reveals the following sequence. MSP is first detectable in the cytosol of spermatocytes during meiotic prophase, specifically in mid-pachytene spermatocytes when other sperm function proteins are first synthesized (Chu and Shakes, 2013; Fig. 1C,D). Then, towards the end of meiotic prophase (karyosome stage), MSP packs into symmetrically elongating structures called fibrous bodies (FBs) (Fig. 1B). These individual FBs develop on the cytosolic surface of Golgi-derived organelles known as membranous organelles (MOs) (Roberts et al., 1986; Fig. 1B). These FBs are filled with parallel 4.5 nm filaments (Roberts et al., 1986) that contrast with the 11 nm diameter filaments involved in sperm motility (King et al., 1994a,b; Bullock et al., 1998). As MSP is synthesized, its localized assembly into FBs promotes both FB growth and MSP sequestration. MSP remains locked in these FB structures through the post-meiotic partitioning process during which FB-MO complexes partition to individual spermatids and away from the central residual body (Fig. 1E). Once spermatids detach from the residual body, the FB-MO complexes disassociate, the MOs dock with the plasma membrane, and the FBs disassemble into MSP dimers (Roberts et al., 1986).

The packing of MSP into FB-MO complexes is hypothesized to both prevent MSP from interfering with the actin- and tubulin-mediated events of meiotic chromosome segregation and cell division (Chu and Shakes, 2013) and facilitate MSP partitioning to spermatids during the post-meiotic budding division (Nishimura and L'Hernault, 2010; Fig. 1E). However, the necessity of MSP sequestration has never been directly addressed. Additionally, little is known about the composition of FBs. They are assumed to consist solely or largely of MSP, but in principle would require their own set of accessory proteins, like those required to mediate MSP-mediated motility.

Here, we identify *spe-18*, a gene identified in a screen for spermatogenesis-defect mutants, as an essential factor in nematode spermatogenesis and FB assembly. In the absence of SPE-18, MSP fails to assemble into FBs, and no haploid sperm are produced as the developing spermatocytes arrest without undergoing proper meiotic divisions. We show that the *spe-18* gene encodes an intrinsically disordered protein, the subcellular localization pattern of which within wild-type and mutant spermatocytes suggests that it functions to both localize and structure FB assembly.

RESULTS

spe-18(hc133) spermatocytes arrest as undivided spermatocytes

Until recently, the only factor known to be required for the initial assembly of MSP into FBs was the ser/thr kinase SPE-6. In *spe-6* mutant spermatocytes, MSP remains cytosolic, and spermatocytes arrest development without completing their meiotic divisions or undergoing cytokinesis (Varkey et al., 1993; Muhlrad and Ward, 2002; Fig. 2A). More recently, the early-acting spermatogenesis-specific transcription factor *spe-44* (Kulkarni et al., 2012; Fig. 2A) was found to have defects in FB assembly. Notably, both have

Development (2021) 148, dev195875. doi:10.1242/dev.195875

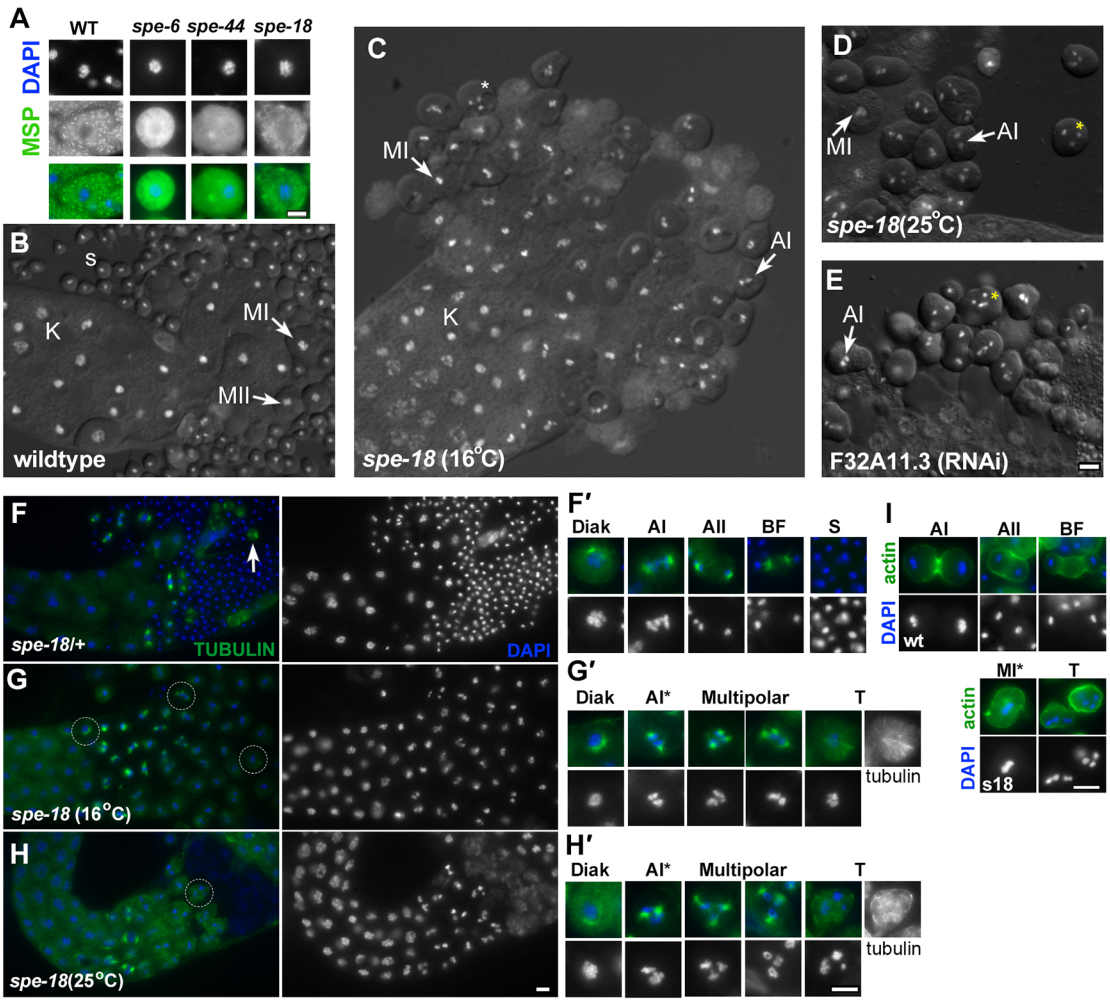

Fig. 2. *spe-18* spermatocytes are defective in FB assembly and progression through the meiotic divisions. (A) Wild-type (WT) and mutant spermatocytes co-labeled with DAPI (blue) and anti-MSP (green). (B-E) DIC/Hoechst image of wild-type (B), *spe-18* at 16°C (C) and 25°C (D), and F32A11.3 (RNAi) (E) sperm spreads. Yellow asterisks mark arrested spermatocytes with three or four compact chromosome masses. (F-H) Proximal region of isolated male gonads from heterozygous and homozygous *spe-18* males raised at the indicated temperature and labeled with DAPI (blue) and anti-tubulin (green). (F′-H′) Magnified images of staged spermatocytes either from the same worms (encircled cells in G,H) or sibling worms. (I) Isolated spermatocytes from wild-type and *spe-18* males labeled with DAPI (blue) and Alexa 488-phalloidin (green). AI, anaphase I; AII, anaphase II; BF, budding figure; Diak, diakinesis; K, karyosome; MI, metaphase I; MII, metaphase II; S, haploid spermatids; T, terminal arrest. Aberrant meiotic forms are indicated with asterisks. Scale bars: 5 µm.

defects in FB assembly and arrest as undivided spermatocytes with defects in meiotic chromosome segregation.

To identify other factors required for the assembly of MSP into FBs, we examined other spermatocyte arrest mutants. *spe-18(hc133)*, previously annotated as *spe-7* (Kulkarni et al., 2012; Chu and Shakes, 2013), was originally isolated in a screen for spermatogenesis-defective mutants by D. Shakes and S. L'Hernault. To characterize *spe-18(hc133)*, we first confirmed that they exhibited the standard characteristics of SPE mutants; namely, that mutant hermaphrodites produce few or no self-progeny but produce cross-progeny when mated to wild-type males (L'Hernault et al., 1988; Nishimura and L'Hernault, 2010). This result indicates that sperm, not oocytes, are responsible for the fertility defect. To determine whether the mutation was temperature sensitive, we analyzed the self-fertility of mutant hermaphrodites at three temperatures (Table 1). Control hermaphrodites produced >100 progeny and a small number of unfertilized oocytes. These brood sizes are lower than those of wild type but reflect the lower fertility of both the morphological marker *unc-4* and the *him-8* mutation used to increase the number of males. *spe-18* hermaphrodites produced no embryos and very few unfertilized oocytes. Although most temperature-sensitive mutants exhibit more severe defects at elevated temperatures, the self-fertility of *spe-18* hermaphrodites was mildly sensitive to cold; hermaphrodites were completely infertile at 16°C, but at 25°C individuals laid more unfertilized oocytes and produced as many as eight offspring. Dead embryos were notably absent, suggesting that when fertilization-competent sperm were produced, they generated viable offspring.

Analysis of isolated and flattened male gonads revealed defects in both meiotic chromosome segregation and cytokinesis. Control gonads included spermatocytes at all stages of development including a small number of meiotically dividing spermatocytes and large numbers of round, haploid spermatids (Fig. 2B). In contrast, *spe-18* gonads lacked haploid spermatids but accumulated large numbers of spermatocytes that were the size of primary spermatocytes (Fig. 2C,D). The relative severity of the meiotic chromosome segregation defects was mildly enhanced by cold temperatures. Although most of these chromosome segregation phenotypes were observed at all temperatures, mutant spermatocytes typically arrested a single chromatin cluster at 16°C (Fig. 2C), two chromatin clusters at

Development (2021) 148, dev195875. doi:10.1242/dev.195875

Table 1. Analysis of hermaphrodite self-sterility phenotype

Strain	Temperature (°C)	*n*	Oocytes	Embryos	Hatch rate	Progeny
unc-4; *him-8*	16	8	18.3±5.9	183.8±2.9	87%	160±2.6
	20	9	72.2±4.8	187.9±9.9	90%	170±9.8
	25	7	12.9±2.6	135.1±6.0	73%	99.6±3.3
spe-18 unc-4; *him-8*	16	22	9.6±2.0	0	n/a	0
	20	20	17.05±1.4	0.7±0.2	100%	0.7±0.2
	25	17	47.6±4.3	2.4±0.5	100%	2.4±0.5

Data are shown as mean±s.e.m.
n/a, not applicable.

20°C (data not shown), and three or four chromatin clusters at 25°C (Fig. 2D). When *spe-18* gonads were scored by their predominant spermatocyte arrest phenotype, 16°C males (*n*=45) had mostly single (47%) or double (42%) chromatin clusters whereas 25°C males (*n*=32) had mostly double (44%) or three or four (38%) chromatin clusters.

spe-18(hc133) spermatocytes exhibit diverse cytoskeletal defects

To understand these chromosome segregation defects better, gonads were co-labeled with DAPI and anti-tubulin antibodies (Fig. 2F-H). Both heterozygous (Fig. 2F) and homozygous (Fig. 2G,H) spermatocytes entered M phase and formed meiotic spindles. Heterozygous spermatocytes completed anaphase II and then underwent a budding division (Fig. 2F′) to form haploid spermatids without tubulin (Fig. 2F′) and tubulin-containing residual bodies (Fig. 2F, arrow). *spe-18* spermatocytes always formed metaphase I spindles, and most subsequently formed spindles with four fully or partially separated microtubule asters (Fig. 2G-H′). However, mutant spindles failed to segregate the chromosomes properly. Spermatocytes with multipolar spindles more typically arrested with two or more chromatin masses. *spe-18* differs from previously described SPE mutants in that microtubules within its most terminal (T) spermatocytes reorganize into a unique, polymerized-yet-disorganized pattern.

To understand the cytokinesis defects better (Fig. 2C,D), we next examined actin microfilament patterns (Fig. 2I). Wild-type sperm spreads included anaphase spermatocytes with central actin rings and budding figures with polarized actin patterns as previously observed (Ward et al., 1981; Winter et al., 2017; Hu et al., 2019), but such patterns were never observed in either meiotic or arrested *spe-18* spermatocytes. Instead, their actin remained cortical and uniform. Together, these results suggest that *spe-18* spermatocytes enter M phase and appear to undergo centrosome duplication, but then fail in both normal chromosome segregation and cytokinesis.

Because temperature impacted the severity of the chromosome segregation defects, we examined whether MSP assembly would be similarly affected. Intact gonads from *spe-18* males raised continuously at 16°C or 25°C were compared with gonads from both heterozygous *spe-18*/+ siblings and *spe-6(hc49)* males (Fig. 3). In *spe-18*/+ gonads (Fig. 3A), MSP-labeled FBs were first detectable in late pachytene (P) stage spermatocytes as small globular structures that grew and elongated through the karyosome (K) and meiotic division (D) stage. In *spe-6* gonads (Fig. 3B), MSP remained diffuse throughout the cytosol at all stages. In 16°C *spe-18* gonads (Fig. 3C), MSP failed to assemble into FBs but was not diffuse as in *spe-6* spermatocytes. Within 25°C *spe-18* spermatocytes, MSP structures were more defined; cortical focal planes revealed extended MSP fibers within pachytene and later spermatocytes (Fig. 3D). Thus, whereas MSP within *spe-6* spermatocytes remains unpolymerized (Fig. 3B), MSP within *spe-18* spermatocytes inappropriately polymerizes into long, thin cortical fibers rather than packing into MO-associated, paracrystalline FBs. Importantly, these defects in FB assembly precede the defects in meiotic chromosome segregation.

SPE-18 is conserved in diverse nematodes and is predicted to contain extended intrinsically disordered regions

To explore the molecular role of SPE-18 in spermatogenesis, we first needed to clone the *spe-18* gene. The *hc133* mutation was mapped to a small region of chromosome II; of 43 genes within this interval, only one gene, F32A11.3, had been previously identified in large-scale microarray studies as exhibiting a 'spermatogenesis-enriched' expression pattern (Reinke et al., 2000, 2004). To determine whether the F32A11.3 gene in *spe-18* mutants contained a molecular lesion, we amplified and sequenced the F32A11.3 gene from wild-type and *spe-18(hc133)* worms and found that *hc133* contains a C/T point mutation in the last exon that changes the CAA codon of glutamine (Q301, highlighted in red) to the premature stop codon TAA (Fig. 4A,B).

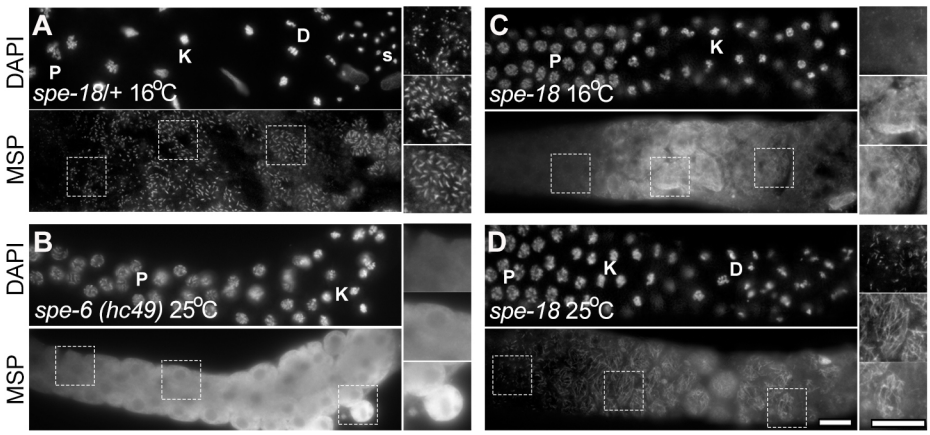

Fig. 3. Alternative MSP patterns in *spe*-6 and *spe-18* mutants. (A-D) Proximal region of isolated male gonads from males raised at the indicated temperature and labeled with DAPI and anti-MSP. Insets show magnified images of the boxed regions adjusted for contrast and brightness. D, meiotic division zone; K, karyosome; P, pachytene; s, spermatids. Scale bars: 10 µm.

Development (2021) 148, dev195875. doi:10.1242/dev.195875

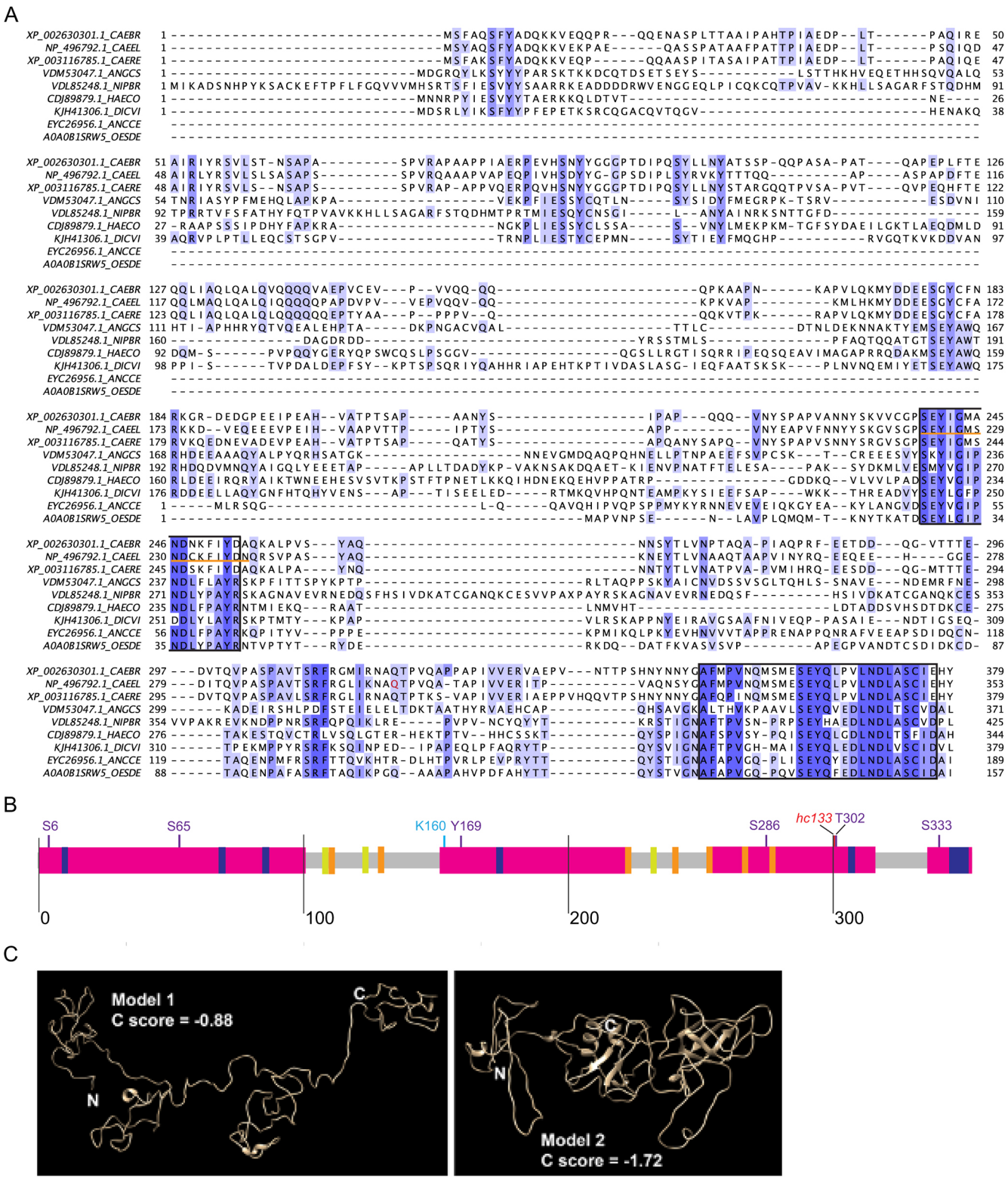

Fig. 4. The amino acid sequence of SPE-18 (F32A11.3) and its bioinformatic analysis. (A) Clustal Omega alignment (Madeira et al., 2019) of F32A11.3 with other nematode species. Residues are colored to reflect percentage identity across species; boxed regions represent regions of high homology. Residues underlined in orange represent the peptide used to generate an antibody (aa 266-279). Species include *Caenorhabditis elegans* (CAEEL), *Caenorhabditis briggsae* (CAEBR), *Caenorhabditis remanei* (CAERE), *Angiostrongylus costaricensis* (ANGCS), *Nippostrongylus brasiliensis* (NIPBR) and *Ancylostoma ceylanicum* (ANCCE) from the order Rhabditida as well as *Haemonchus contortus* (HAECO), *Dictyocaulus viviparus* (DICVI) and *Oesophagostomum dentatum* (OESDE) from the order Strongylida. (B) Diagram of SPE-18 protein with annotations: predicted disordered regions from Phyre2 (PhDo) and PrDOS are shown as magenta boxes (Kelley et al., 2015; Ishida and Kinoshita, 2007); potential phosphorylation sites that are both conserved and predicted with high confidence by NetPhos3.1 (Blom et al., 1999) in purple; ubiquitylation site predicted by UbPred (Radivojac et al., 2010) in light blue; pre-mature stop codon in *hc133* (CAA/TAA, aa 301Q) in red; iTasser structural predictions from model 1 (yellow bars are helices) or model 2 (dark blue bars are helices, orange bars are strands). Black vertical lines mark the exon boundaries. (C) Top two-scoring iTasser models of SPE-18 protein structure.

Development (2021) 148, dev195875. doi:10.1242/dev.195875

To verify that F32A11.3 encoded *spe-18*, we used RNAi feeding to deplete F32A11.3 in *him-8* hermaphrodites and their male progeny. F32A11.3-depleted males exhibited spermatocyte defects that were visually indistinguishable from those of *spe-18(hc133)* males (Fig. 2E). Together, the RNAi, microarray and sequencing results confirmed the molecular identity of *spe-18*. Furthermore, as RNAi knockdowns invariably represent loss-of-function phenotypes, the RNAi phenotype suggests that the truncation of SPE-18 in *spe-18(hc133)* mutants represents a loss-of-function, rather than a neomorphic, phenotype.

spe-18 encodes a 353 amino acid protein (Fig. 4A) that lacks any known functional domains. BLASTP analysis with the full-length sequence identified highly conserved homologs of F32A11.3 within multiple members of the *Caenorhabditis* genus (Fig. 4A). BLASTP analysis of the conserved C-terminal domain revealed homologs in nematode species from the larger Rhabditida order as well as the order Strongylida (Fig. 4A). Alignments to these less-conserved homologs revealed both a central and C-terminal region of extended, high sequence conservation, as well as shorter regions of conservation throughout (Fig. 4A).

Multiple lines of evidence from amino acid composition, bioinformatics and biochemistry suggest that SPE-18 is largely unstructured. The amino acid composition reveals SPE-18 as an acidic protein with an isoelectric point of 4.78. The protein is rich in the disorder-promoting residues proline (P), glutamine (Q), glutamic acid (E) and serine (S), but it also has abundant alanines (A) and valines (V) (Fig. 4A). Bioinformatic studies indicate that SPE-18 lacks transmembrane domains, and two distinct disorder-predicting programs suggest that SPE-18 has large intrinsically disordered regions. Phryre2 (Kelley et al., 2015) predicts that it is 70% unstructured (Fig. 4B). PrDOS (Ishida and Kinoshita, 2007) predicts that SPE-18 contains 25-50% unstructured residues depending on the false positive setting; these amino acids are largely a subset of those identified by Phrye2. In addition, the most likely model predicted by structure modeling program I-TASSER (Roy et al., 2010) suggests that SPE-18 possesses minimal secondary structure (Fig. 4B,C). In this context, it is notable that both I-TASSER model 2 and PSSpred (Yan et al., 2013) predict that the conserved C-terminal domain contains a ten amino acid alpha helix (Fig. 4B,C). Furthermore, when this C-terminal region is deleted in *hc133* mutants, the truncated protein is destabilized (Fig. 5A,C). Finally, another biochemical property of intrinsically unstructured proteins is that they typically remain soluble in heated solutions (Uversky, 2017). To test this property, we expressed recombinant SPE-18 in *Escherichia coli* and then assayed whether SPE-18 within the resulting lysate remained in the supernatant after a 10-min heat treatment at 95°C. Under these conditions, most proteins within the lysate precipitated whereas SPE-18 remained in the supernatant (Fig. S1). Collectively, these data predict that SPE-18 functions as an intrinsically disordered protein.

As the function of intrinsically unstructured proteins is often regulated by post-translational modifications (PTMs), we also employed bioinformatic approaches to assess potential PTMs. NetPhos 3.1 predicted several high confidence phosphorylation sites in SPE-18 that are also conserved in its *Caenorhabditis* homologs (Fig. 4B, highlighted in purple) and two (S6 and Y169) that are conserved in more distant species. UbPred predicted a single, high-score ubiquitylation site (K160, highlighted in light blue).

Together, these data predict that SPE-18 functions as a protein with large intrinsically disordered regions. Notably, the SPE-18 sequence also includes both extended and shorter conserved regions that could potentially serve as sites for molecular interactions or regulation by post-translational modifiers.

SPE-18 protein localizes in a stage-specific pattern to FBs of developing spermatocytes

To understand how SPE-18, as an unstructured protein, promotes the assembly of MSP into FBs, we next sought to determine the cellular distribution of SPE-18. Does SPE-18 direct localized MSP assembly as a resident protein of either the FB or MOs, or does SPE-18 direct FB assembly from some other cellular compartment? Is SPE-18 only present in spermatocytes or might it also be present in haploid sperm such that it could regulate MSP function at multiple stages of spermatogenesis?

To address these questions, we first generated polyclonal antisera to a region of SPE-18 that was predicted to be both antigenic and specific (Fig. 4A). Because the antigenic sequence is before the *hc133* truncation, the antibody was predicted to recognize both the full-length and truncated protein. Western blots were used to test the specificity of the anti-SPE-18 antibody (Fig. 5A). Anti-SPE-18 antibody bound to a 42 kDa protein in lysates of wild-type adult males but not in *spe-18(hc133)* males or males lacking an essential transcription factor for *spe-18*, SPE-44 [*spe-44(ok1400)*; Kulkarni et al., 2012; Fig. 5A]. This result not only confirmed the specificity of the antibody but also revealed that the *hc133* allele that lacks the conserved C-terminal domain is functionally null as no truncated protein could be detected in the *hc133* sample.

On the same western blot, we tested hermaphrodite samples from specific larval stages (Fig. 5A) and found that the major band detected in adult males could only be detected in fourth stage larvae (L4), the only stage when hermaphrodites are actively producing sperm. The notable absence of SPE-18 in adult hermaphrodites that have spermatozoa in their spermathecas suggested that SPE-18 might function in developing and/or meiotically dividing spermatocytes but not in haploid sperm.

We next determined the subcellular localization of SPE-18 by co-labeling isolated wild-type and mutant male gonads with DAPI and anti-SPE-18 antibody. Within wild-type male gonads, SPE-18 labeling was first detectable in late pachytene spermatocytes and then increased in intensity through the karyosome stage (Fig. 5B). Despite the non-specific bands in the western blots, antibody binding was not above background in either *spe-18(hc133)* (Fig. 5C; Fig. S2C, D) or *spe-44* (Fig. S2E,F) gonads, confirming the specificity of the antibody for immunocytology. Within developing spermatocytes, SPE-18 labeled numerous discrete structures the pattern and distribution of which seemed similar to FBs (Fig. 5B). SPE-18 labeling then decreased in intensity through the meiotic divisions and became undetectable in haploid spermatids. This failure to detect SPE-18 in haploid sperm was consistent with the absence of a SPE-18 signal in western blots of adult spermatozoa-containing hermaphrodites. Importantly, as the one key defect in *spe-18(hc133)* spermatocytes is the inability to assemble MSP into FBs, clear evidence of SPE-18 localizing to FBs might suggest a direct role for SPE-18 in FB assembly.

If SPE-18 contributes to the localization and/or nucleation of FB assembly, then SPE-18 should localize to developing FBs before MSP. To test this prediction, we compared the localization patterns of SPE-18 and MSP (Fig. 5D,E) and discovered previously undescribed details of FB growth and morphogenesis. In late pachytene spermatocytes when SPE-18 became detectable in distinct, spherical ‘pre-FB’ structures, MSP was already present but diffuse throughout the cytoplasm. By diplotene, when spermatocytes are transitioning from pachytene to the karyosome stage, MSP

Development (2021) 148, dev195875. doi:10.1242/dev.195875

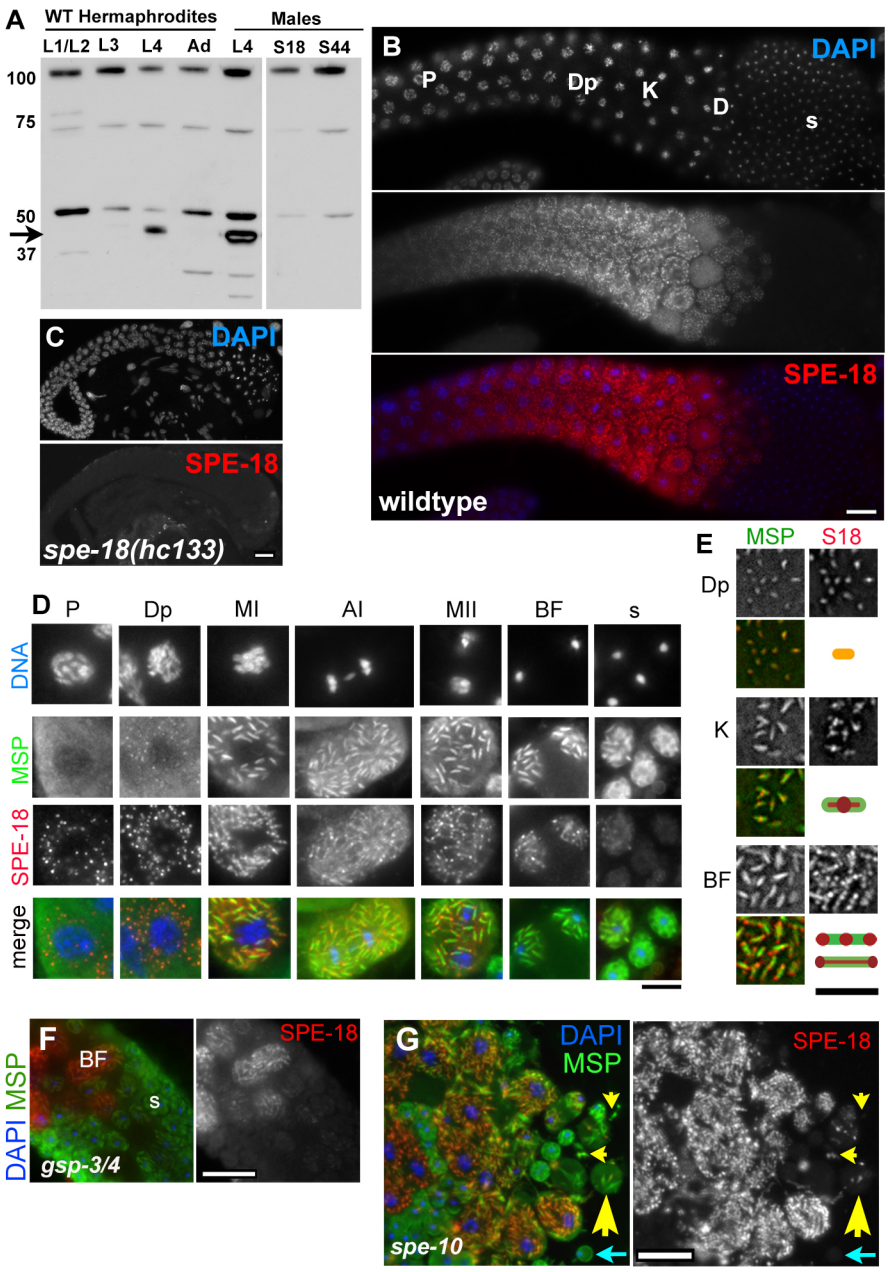

Fig. 5. SPE-18 localizes to developing FBs in a stage-specific pattern. (A) Western blot comparing SPE-18 levels in age-synchronized wild-type hermaphrodites, wild-type males, and mutant *spe-18* (S18) and *spe-44* (S44) males. A non-specific band at ~100 kDa serves as a loading control. Arrow shows the position of SPE-18 with strong bands in L4 hermaphrodites and males. (B,C) Isolated male gonads co-labeled with DAPI and anti-SPE-18 antibody in wild-type males (B) or *spe-18*(*hc133*) males (C). (D-G) SPE-18/MSP co-immunolabeling in wild-type and mutant spermatocytes and spermatids. (D) Epifluorescence images. (E) Multi-dimensional deconvoluted images and schematics showing SPE-18 (red) and MSP (green), and overlap (yellow). (F) Stabilized FBs in *gsp-3/4* spermatids contain MSP but not SPE-18. (G) MSP and SPE-18 patterns in *spe-10* sperm spreads containing FBs mis-segregated to a residual body (large yellow arrowheads), FB cytoplasts (small yellow arrowheads) and spermatids (cyan arrows). AI, anaphase I; BF, budding figure; D, meiotic division zone; Dp, diplotene; K, karyosome; MI/II, metaphase I/II; P, pachytene; s, spermatids. Scale bars: 10 µm (B,C,F,G); 5 µm (D,E).

colocalized in spherical structures with SPE-18. Through the karyosome stage, the SPE-18 and MSP patterns began to diverge (Fig. 5E). In meiotically dividing spermatocytes, MSP assemblages grew primarily through elongation at the two ends but remained uniformly distributed throughout the FBs. In contrast, SPE-18 became enriched at the two ends with the remaining SPE-18 present in either an additional central accumulation or in a barbell-like pattern with central interconnecting stripe. During the budding division that follows anaphase II, SPE-18 partitioned to the spermatids and away from the central residual body. Yet SPE-18 labeling was undetectable in all but the most recently individualized spermatids. FB-packaged MSP partitioned to the spermatids and then, as FBs disassembled during the spermatid maturation process, MSP dispersed throughout the cytoplasm. The localization of SPE-18 to pre-FB structures and its subsequent enrichment in regions of FB growth are consistent with SPE-18 functioning to either localize MSP polymerization and/or promote the gathering and bundling of MSP filaments.

During the process of spermatogenesis, cellular components that are no longer needed are typically discarded into the residual body during the post-meiotic budding division (Fig. 1F). Thus, we were surprised by the unusual pattern of SPE-18 partitioning to the spermatids and then becoming undetectable shortly thereafter (Fig. 5B,D). To rule out the possibility that this apparent SPE-18 loss was an artifact of antigen accessibility, we assessed the relative levels of MSP and SPE-18 in aging celibate males (Fig. S3). The western blot of sibling males supported our immunocytology results; as males accumulated spermatids, their MSP levels increased whereas their SPE-18 levels decreased in proportion to the shrinking numbers of late-stage spermatocytes. This result indicates that SPE-18 is indeed degraded in newly individualized spermatids.

SPE-18 localization to and subsequent loss from the ends of mature FBs suggested that SPE-18 might protect FBs from disassembly during the meiotic divisions. To test this hypothesis, we examined the localization of SPE-18 in the P1 phosphatase mutant *gsp-3/4*, in

Development (2021) 148, dev195875. doi:10.1242/dev.195875

which spermatids retain stable FBs (Wu et al., 2012). However, within *gsp3-4* sperm, SPE-18 loss occurred on schedule, shortly after the spermatids detached from residual bodies (Fig. 5F). Thus, although SPE-18 loss may be necessary for FB disassembly, its loss is clearly not sufficient. Instead, our results lend support to the proposal that GSP-3/4 promotes MSP disassembly (Wu et al., 2012).

The rapid disappearance of SPE-18 following sperm individualization raised the question of what regulates the stability of SPE-18 itself. SPE-18 loss coincides with two cellular transitions that might regulate its degradation: (1) physical separation of FBs from their associated MOs and (2) physiological differences between spermatocytes and haploid spermatids. To address these possibilities, we examined a mutant of *spe-10*, a palmitoyl transferase that is required for proper partitioning of FB-MOs into spermatids (Shakes and Ward, 1989; Gleason et al., 2006). In *spe-10(hc104)* spermatocytes, FBs separate from their MOs prior to spermatid-residual body separation, and a subset of MO-separated FBs either mis-segregate to the residual bodies or form cytoplasts that bud directly from the residual bodies (Fig. 5G). SPE-18 proved stable within spermatocytes in which FBs had separated from their MOs. Furthermore, of the *spe-10* FBs that mis-segregated to residual bodies, most (40/50) were labeled with both MSP and SPE-18 antibodies (large yellow arrowhead). Conversely, SPE-18 was consistently undetectable in *spe-10* spermatids (cyan arrow), and of the FBs that were released in the anomalous form of independent cytoplasts, only some were labeled with SPE-18 antibody (small yellow arrowheads). Thus, SPE-18 loss is not linked to FB-MO separation. Instead, these observations suggest that SPE-18 loss is coupled to a property of individualized spermatids and *spe-10* cytoplasts that is associated with their separation from residual bodies or the mutant spermatocytes, respectively.

SPE-18 foci form in association with developing MOs

Because FBs develop in close association with the Golgi-derived MOs (Fig. 1B), it can be challenging to distinguish between the two compartments. To examine the relationship between SPE-18 and MOs, we compared the localization patterns of SPE-18 to the MO marker 1CB4 (Okamoto and Thomson, 1985), a monoclonal antibody that labels multiple MO glycoproteins (Fig. 6A). Would SPE-18 foci become detectable before or after a marker of the Golgi-to-MO conversion? Would SPE-18 patterns ultimately diverge from the 1CB4 pattern as predicted if SPE-18 is a component of the FB rather than the MO? Within developing pachytene and karyosome stage spermatocytes (Fig. 6A), the first detectable SPE-18 structures were adjacent or within the 1CB4-labeled foci, consistent with the known ultrastructure of FB-MO complexes (Roberts et al., 1986; Figs 1A, 6A). However, in meiotically dividing spermatocytes, when SPE-18 developed the multi-point or barbell pattern, the patterns diverged. The small size of the FB-MO limited what could be deduced regarding the relationship of the two patterns. However, enlarged and contrast-enhanced images (Fig. 6A) are consistent with the hypothesized schematic shown. SPE-18 associates with MOs during the earliest stages of FB development; and yet the manner in which the MO and SPE-18 patterns diverge are consistent with SPE-18 being an early component of FBs rather than MOs.

In the absence of the kinase SPE-6, SPE-18 still forms nascent pre-FB structures

Because both SPE-18 and the kinase SPE-6 are required for MSP to assemble into FBs, we investigated whether and how SPE-18 localization patterns might change when MSP uniformly distributes throughout the cytoplasm as in *spe-6(hc49)* mutants (Fig. 3B). In heterozygous *spe*-6/+ gonads, the MO and SPE-18 patterns were indistinguishable from those of wild type (Fig. 6B). In developing *spe-6(hc49)* spermatocytes (Fig. 6C), SPE-18 initially localized to discrete 1CB4-labeled 'pre-FB' structures that were largely indistinguishable from their heterozygous counterparts. However, these structures could only be first detected in later karyosome stage spermatocytes (Fig. 6C). This apparent delay may reflect a limit in detecting smaller SPE-18 foci or a synergistic interaction with other FB components or SPE-6 itself. As *spe-6* spermatocytes progressed toward their terminal pro-metaphase arrest state (Varkey et al., 1993), these SPE-18 structures grew in size but remained as single spherical masses; they did not appreciatively extend or restructure into the multi-point or barbell structures observed in wild-type spermatocytes (Figs 5D,E, 6C). These results suggest that SPE-18 associates with developing MOs independently of SPE-6. However, SPE-6 is subsequently required either directly or indirectly for MSP and possibly other FB components to add to these pre-FBs. In the absence of normal FB assembly and elongation, SPE-18 fails to structurally reorganize from its initially spherical foci.

DISCUSSION

For cells to function properly, polymerization of their cytoskeletal elements must be precisely controlled in both time and space. For many cells, localized polymerization and/or cytoskeletal assembly is essential to initiate new cell functions. For nematode spermatocytes, localized MSP polymerization is hypothesized to both package MSP for post-meiotic partitioning and sequester it from interfering with the meiotic divisions. In the present study, we show that the spermatogenesis-specific protein SPE-18 promotes the localized assembly of the nematode major sperm protein MSP into tightly packed, paracrystalline structures known as FBs. *spe-18* mutants exhibit sperm-specific sterility, and spermatocytes are unable to assemble MSP into FBs; instead, MSP assembles into long, thin cortical fibers, particularly at elevated temperatures (Fig. 3). Our studies reveal an important distinction between the kinase SPE-6, which is required for MSP polymerization, and SPE-18, which is required to localize MSP assembly at the MOs. Consistent with this model (Fig. 7), SPE-18 is present in the right place at the right time. In wild-type spermatocytes, SPE-18 forms spherical 'pre-FBs' in association with developing MOs (Fig. 6), and these pre-FBs form before MSP colocalizes to these structures (Fig. 5). SPE-18 localizes to the MOs independently of SPE-6, but without SPE-6 MSP fails to join the pre-FBs. Conversely, with SPE-6 but without SPE-18 MSP polymerizes into fibers that are neither localized to the MOs nor constrained by the structural parameters of normal FB assembly.

spe-18 spermatocytes exhibit additional defects in both meiotic chromosome segregation and cytokinesis. Given the SPE-18 localization patterns and MSP phenotype, we believe that that these defects are an indirect secondary consequence of non-localized MSP polymerization. It is easy to envision cortical MSP polymers interfering with both the anaphase pulling forces of astral microtubules and the actin reorganization events of contractile ring and residual body formation. Such disruptions would lead to the observed defects in chromosome segregation, failed cytokinesis, and the formation of multi-aster spindles.

These disruptions of the actin and tubulin cytoskeleton demonstrate the necessity of MSP sequestration, but why assemble larger FB structures rather than sequester monomers or dimers like actin and tubulin? Spermatocyte arrest mutants including *spe-10* (Nishimura and L'Hernault, 2010) suggest that FBs promote the reliable, asymmetric partitioning of MSP into spermatids as

Development (2021) 148, dev195875. doi:10.1242/dev.195875

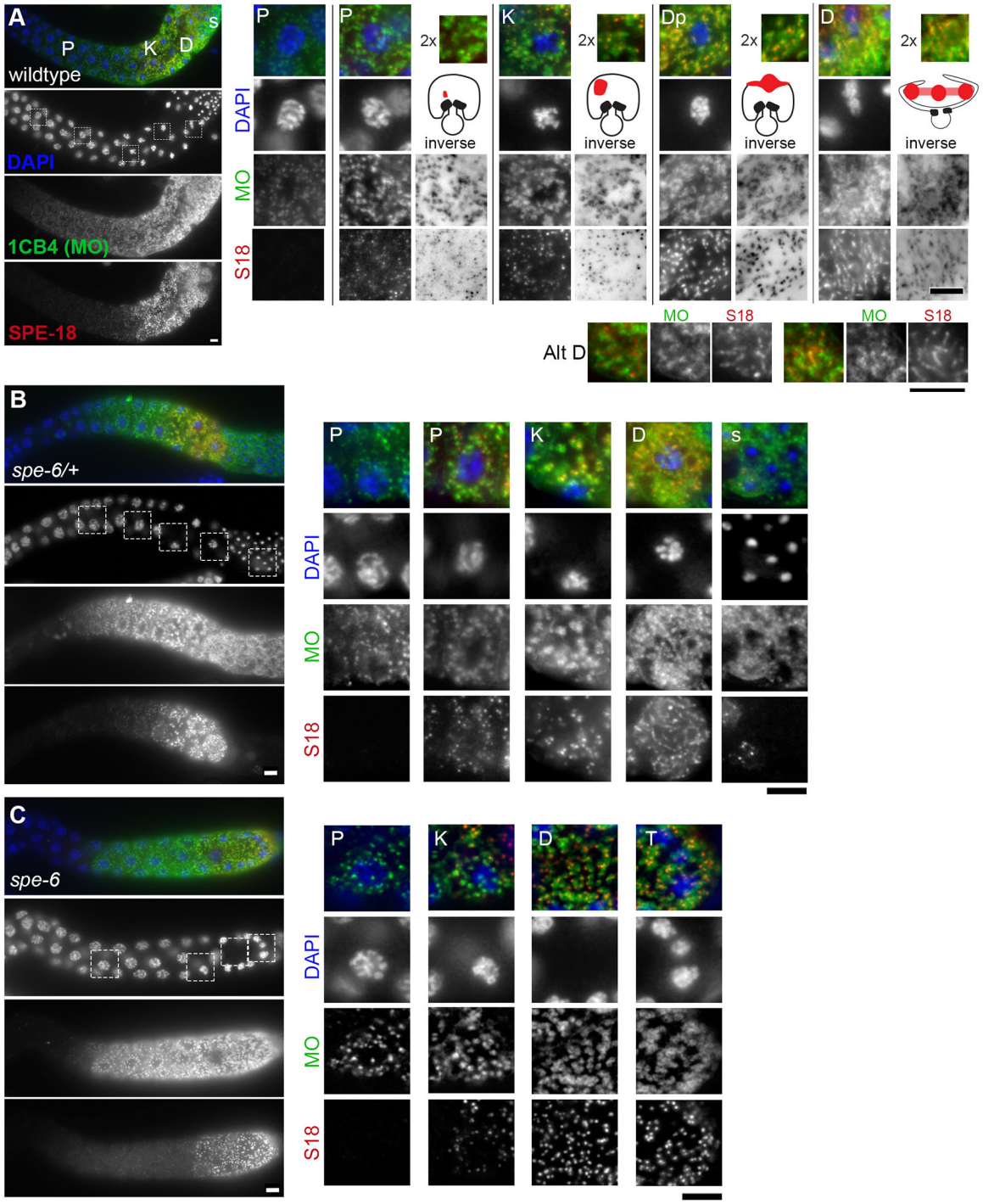

Fig. 6. MO and SPE-18 patterns in wild type and *spe-6(hc49)*. (A-C) Co-immunolabeling of wild-type (A), heterozygous (B) and *spe-6* (hc49) (C) gonads with DAPI (blue), anti-SPE-18 (red) and the MO marker 1CB4 (green). (A) Proximal wild-type gonad and enlarged single-channel images from the indicated regions. Line drawings of the FB-MO complex shows the hypothesized relationship based on Fig. 5 and published immune-electron microscopic images (red represents SPE-18; Roberts et al., 1986). Inverted MO and SPE-18 images and contrast-enhanced enlarged merge images are also shown. Regions of alternative dividing (Alt D) spermatocytes are enlarged and contrast enhanced. (B,C) SPE-18 associates with MOs in both *spe-6*/+ (B) and *spe-6(hc49)* (C) male gonads and enlarged single-channel inserts. Stages include pachytene (P), diplotene (Dp), karyosome (K), meiotic divisions (D), spermatids (s) and terminal (T) prometaphase arrest. Scale bars: 5 µm.

partitioning soluble MSP dimers would be far less efficient. MSP sequestration may also prevent premature MSP signaling of oocyte maturation (Miller et al., 2001) and ensure that such signals come only from activated sperm.

Our characterization of SPE-18 localization patterns suggests a new model of FB assembly (Fig. 7): (1) SPE-18 forms spherical pre-FBs at each MO that function as general gathering sites for MSP filaments; (2) in a process that requires the kinase SPE-6, MSP or MSP filaments are then recruited to these pre-FBs; (3) as MSP levels increase and MSP concentrates at these sites, MSP filaments bundle into FBs; (4) as FBs continue to develop, SPE-18 shifts to a multi-point pattern that promotes ongoing FB elongation at the two ends

Development (2021) 148, dev195875. doi:10.1242/dev.195875

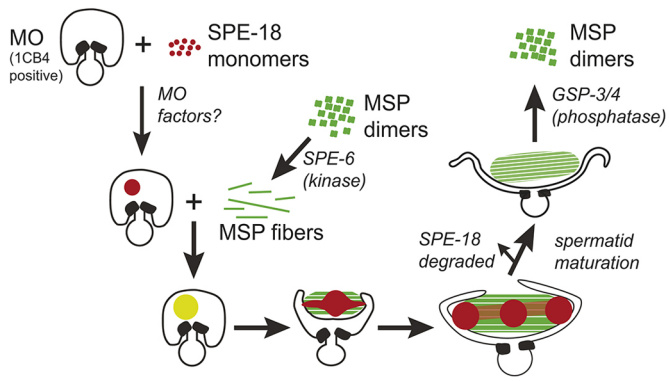

Fig. 7. Model of SPE-18 function in localized FB assembly. Developing MOs (distinguished as 1CB4-positive structures) can be first detected in early to mid-stage pachytene spermatocytes. SPE-18 proteins are recruited to form MO-associated foci (pre-FBs) in mid to late-stage pachytene spermatocytes. As MSP levels increase, MSP will form polymers when SPE-6 is present. When both SPE-6 and SPE-18 are present, MSP polymerization (or the gathering of MSP polymers) is localized to pre-FBs. As FBs grow and extend, SPE-18 forms a barbell or multi-point pattern that is distinct from the spindle-shaped MSP structure. Following the post-meiotic separation of spermatids from a central residual body, SPE-18 is degraded, FBs are released from their associated MO, and the phosphatase GSP-3/4 mediates the disassembly of polymerized MSP into dimers.

and expansion in the middle, a distribution that correlates with the formation of spindle-shaped FBs; (5) as SPE-18 further concentrates at the two ends, FBs elongate without expanding substantially in width. In this model, SPE-18 both nucleates localized MSP assembly and subsequently shapes the growing FBs by localizing the regions of expansion.

Prior to this study, the only known component of FBs was MSP itself. The discovery that the SPE-18 localization patterns change as the FBs develop reveals previously unappreciated complexities in FB composition, growth and shaping. SPE-18 not only localizes MSP assembly to the FBs, but, as FBs develop, SPE-18 shifts to a multi-point pattern that is distinct from the spherical to spindle-shaped transition of the MSP pattern (Figs 5 and 7). We hypothesize that this changing SPE-18 distribution promotes FB growth and shapes the MSP assemblage. Alternatively, SPE-18 patterns may change as a passive response to the elongation and bundling of the underlying MSP polymers. SPE-18 clearly localizes MSP assembly. Yet to be determined is whether SPE-18 recruits MSP as dimers or small polymers and whether it is SPE-18 or MSP that directs FB growth.

This study raises new questions regarding both FB composition and control of MSP polymerization. We predict that SPE-18 interacts with multiple binding partners, including diverse FB components and factors that recruit and/or anchor SPE-18 to the MO surface. Although MSP polymerizes differently during FB growth and pseudopod treadmilling, it remains unclear whether this involves distinct or overlapping co-regulators. SPE-18 itself is specific to FBs, but other components may function in both contexts. Proteins known to regulate MSP polymerization in the pseudopods of *Ascaris* sperm (Roberts and Stewart, 2012) may also mediate FB assembly. Candidate interactors should also exist amongst the genes regulated by SPE-44, the transcriptional factor that regulates *spe-18* expression (Kulkarni et al., 2012), and NHR-23, a transcription factor that regulates additional genes required for FB assembly (Ragle et al., 2020).

SPE-18 functions in spermatocytes but is subsequently lost. Rather than being discarded in the residual body, SPE-18 degrades shortly after it partitions to the sperm, and the sperm separate from the residual body. How SPE-18 is lost remains unclear. We discovered that SPE-18 can be stabilized if it mis-segregates to residual bodies or is trapped within arrested spermatocytes (Fig. 5G). Post-translational or pH changes associated with spermatid separation from the residual body likely trigger SPE-18 to disassociate from its binding partners, assume a fully unstructured state, and be subject to proteolytic degradation. The SPE-18 sequence includes several potential phosphorylation sites (Fig. 4), and *Ascaris* spermatocytes are known to maintain a higher pH (6.8) than spermatids (6.2) (King et al., 1992; King et al., 1994a). Many intrinsically disordered proteins become proteolytically sensitive when released from their binding partners (Uversky, 2017; Flock et al., 2014). A distinct question is why SPE-18 is rapidly degraded following sperm individualization. SPE-18 degradation may be essential for both FB disassembly and subsequent sperm function. However, SPE-18 loss is insufficient for FB disassembly; as FB disassembly requires the phosphatases GSP-3/4 (Figs 5F and 7; Wu et al., 2012).

The SPE-18 sequence provides important clues regarding how SPE-18 could promote FB assembly. SPE-18 is predicted to contain extended intrinsically disordered regions, particularly in the first half of the protein (Fig. 4). SPE-18 also contains multiple, smaller conserved regions and two extended, highly conserved regions that are not predicted to be disordered. These could serve as either binding motifs or sites for PTMs. Although the intrinsically disordered regions of SPE-18 are undoubtably crucial for its function, they are not sufficient. In the absence of the mostly structured C terminus, the truncated *hc133* version of SPE-18 is both non-functional and unstable. Proteins with a mix of extended disordered and small structured regions often scaffold the assembly of molecular complexes. Their inherent flexibility paired with multiple high-specificity, low-affinity binding sites enables them to bind to multiple proteins and exist in multiple distinct conformations (Pancsa and Fuxreiter, 2012). Furthermore, their ability to transition rapidly between extended and compact conformations enable some to employ a ‘fly-casting’ mechanism to concentrate binding partners. Examples of such proteins include both the actin-modulator Wiskott–Aldrich syndrome protein (WASP) that links cell signaling to localized actin assembly and the phosphatase Calcineurin whose structure facilitates its multi-faceted regulation (Kim et al., 2000; Creamer, 2013). Disordered regions of proteins often become ordered upon binding to structured proteins (Dyson and Wright, 2002), but can also remain ‘fuzzy’ and never completely fold (Sharma et al., 2015).

Although many proteins with large intrinsically disordered regions function as singlets to interact with multiple, non-self, binding partners, others gather together in large assemblages through liquid phase condensation (Shin and Brangwynne, 2017). Within such assemblages, intrinsically disordered proteins may themselves transition from a liquid to solid/amyloid state as they concentrate over time. Alternatively, intrinsically disordered proteins can form liquid droplets within which other proteins, including highly structured proteins, concentrate and polymerize. Examples of this supportive role include the spatial coordination of microtubule nucleation by BuGZ (Jiang et al., 2015), Tau (Hernández-Vega et al., 2017), PLK4 (Montenegro Gouveia et al., 2018) and TPX2 (King and Petry, 2020). Notably, the patterns of these protein condensates in association with polymerizing microtubules resembles the patterns we observed of SPE-18 interacting with MSP fibers (Figs 5D,E and 7). In a further parallel, when actin filaments bundle in association with the long flexible cross-linker filamin, the form of the resulting actin superstructures (spheres, spindles or elongated rods) can be predictably modulated by the filamin-actin ratios (Weirich et al.,

Development (2021) 148, dev195875. doi:10.1242/dev.195875

2017). Convincing evidence that SPE-18 promotes localized MSP assembly through the process of phase separation awaits both *in vitro* studies and an expanded parts list of FB components. However, these intriguing similarities raise the exciting possibility that MSP will join actin and tubulin in the list of cytoskeletal proteins that employ liquid phase condensation to support their localized assembly.

Together, these studies provide new insights into the process and regulation of FB assembly. They place SPE-18 in the context of other known MSP regulators and reveal SPE-18 as an assembly factor involved in the localized assembly of FBs. Just as studies of MSP assembly/disassembly within the pseudopods of crawling spermatozoa have both challenged and deepened our understanding of actin-based cell motility (Roberts and Stewart, 2012), studies of FB assembly/disassembly dynamics promise to provide an equally informative parallel to our understanding of bundled cytoskeletal structures and their localized assembly. In particular, a deeper understanding of FB dynamics promises to reveal insights into the construction of cytoskeletal assemblages that are facilitated by proteins with large intrinsically disordered regions.

MATERIALS AND METHODS

Strains and culture

Caenorhabditis elegans were cultured on MYOB plates (Church et al., 1995) inoculated with *E. coli* strain OP50, using methods similar to those described by Brenner (1974).

Unless otherwise indicated, the following strains were provided by the CGC, which is funded by NIH Office of Research Infrastructure Programs (P40 OD010440): N2 (Bristol); CB4856 (Hawaiian); CB1489 *him-8(e1489)* IV; BA606 *spe-6(hc49) unc-25(e156) III; eDp6*; BA782 *spe-10(hc104) him-5(e1490)* V; DR103 *dpy-10(e128) unc-4(e120)* II; JK816 *fem-3(q20gf)* IV; SL48 *dpy-5(e61) spe-4(q347)/sDf5 I*; VT132 *sqt-1(sc13) lin-29(n833) / mnC1* [*dpy-10(e128) unc-52(e444)*] II.

SL262 *unc-4(e120) spe-18(hc133) / mnC1* [*dpy-10(e128) unc-52(e444)*] II was originally isolated in an ethyl methanesulfonate mutagenesis screen for SPE mutants by D.C.S. and S. L'Hernault (Department of Biology, Emory University, Atlanta, GA, USA).

DS175 *unc-4(e120) spe-18(hc133)/mnC1* [*dpy-10(e128) unc-52(e444)*] II; *him-8(e1489)* IV was constructed in the D.C.S. lab.

DS176 *rol-1(e91) spe-18(hc133) / mnC1* [*dpy-10(e128) unc-52(e444)*] II; *him-8(e1489)* IV was constructed in the D.C.S. lab.

RV120 *spe-44(ok1400) dpy-20(e1282)/ let-92(s677) unc-22(s7)* IV was a gift from Harold Smith (NIDDK/NIH, USA).

XC26 *gsp-3(tm1647) gsp-4(y418)*/hT2[*bli-4(e937)let-?(q782)*qIs48] I; *him-8(e1489)* IV was a gift from Diana Chu (Department of Biology, San Francisco State University, CA, USA).

Fertility analysis

The number of self-progeny for *unc-4*; *him-8* (wild-type controls) and *spe-18 unc-4*; *him-8* mutants was determined by placing single worms on separate culture plates and transferring them to fresh plates daily to assess the entire brood.

Molecular biology, identification and analysis of the *spe-18* gene

The position of the *spe-18* gene was determined using standard linkage mapping (Sulston and Hodgkin, 1988) and single nucleotide polymorphism (SNP) mapping (Swan et al., 2002) (see Table S1). *hc133* was mapped to linkage group II and to the right of *rol-1*. SNPs that generated restriction fragment length polymorphisms [SNIP-SNPs between N2 and Hawaiian (H) strains] were used to further position on the physical map. N2/H hybrids were generated by crossing *rol-1(e91) spe-18(hc133)* homozygous hermaphrodites to wild-type Hawaiian males. Rol Non-Spe recombinant offspring from the hybrid worms were isolated and lines were established. Lysates from 18 individual lines and SNP analysis was carried out by PCR amplification using specific primers in the region of the SNP followed by restriction digestion using specific enzymes. Data from this analysis positioned *spe-18* to the right of pkp2112 and close to pkp2116 at approximately 13,330 kb. Of the spermatogenesis-enriched genes on linkage group II, F32A11.3 mapped closest to this region.

To identify the molecular lesion in the *spe-18*, the F32A11.3 sequence on WormBase was used to design primer sets to amplify 500 bp overlapping bidirectional sections. PCR-based sequencing was used to sequence F3211.3 from *hc133* mutant DNA in both directions.

For the RNAi experiments, culture plates were soaked with IPTG solution overnight before adding concentrated *E. coli* containing the F32A11.3 feeding construct. Wild-type L4 hermaphrodites were plated on RNAi plates and allowed to lay embryos for 24 h. The F1 progeny were maintained on these plates and then L4 males were transferred to fresh RNAi plates for an additional 24-48 h before analysis.

Immunocytochemistry

To generate anti-SPE-18 antibodies, rabbits were initially pre-screened to identify those whose sera lacked cross-reactivity with *C. elegans* male germlines. Selected rabbits were injected with synthesized peptide corresponding to amino acids 266-279 (YenZym). After a booster injection, serum was collected, and antibodies were affinity purified.

Intact gonads were obtained by dissection of individual males in 5-10 µl of sperm media (50 mM HEPES, 25 mM KCl, 1 mM $MgSO_4$, 45 mM NaCl and 5 mM $CaCl_2$, pH 7.8) on ColorFrost Plus slides (Thermo Fisher Scientific) coated with poly-L-lysine (Sigma-Aldrich). Samples were freeze-cracked in liquid nitrogen. Sperm spreads to analyze detached spermatocytes and spermatids were obtained by applying slight pressure to the coverslip before freeze-cracking. Samples were fixed overnight in −20° C methanol. Specimen preparation and antibody labeling followed established protocols (Shakes et al., 2009). Primary antibodies included: 1:1250 rabbit anti-SPE-18; 1:600 4D5 mouse anti-MSP monoclonal (Kosinski et al., 2005) and 1:50 1CB4 monoclonal (Okamoto and Thomson, 1985). All samples were incubated with primary antibodies for 2 h at room temperature. Affinity-purified secondary antibodies included 1:100 TRITC-conjugated goat anti-rabbit IgG (Jackson ImmunoResearch Laboratories) and 1:100 FITC- or DyLight-conjugated goat-anti-mouse IgG (H+L) (Jackson ImmunoResearch Laboratories). In some experiments, appropriately diluted working solutions of the secondary antibodies were preadsorbed with a powder made from acetone-fixed *C. elegans* (Miller and Shakes, 1995). For actin labeling, dissected gonads were fixed in 4% paraformaldehyde and labeled with Alexa 488-conjugated phalloidin (Cytoskeleton, Inc.) according to established protocols (Winter et al., 2017).

Final slides were mounted with DAPI-containing Fluoro Gel II mounting medium (Electron Microscopy Sciences). Images were acquired under differential interference contrast (DIC) or epifluorescence using an Olympus BX60 microscope equipped with a QImaging EXi Aqua CCD camera. Photos were taken, merged and exported for analysis using the program iVision. For multi-dimensional imaging, *z*-axis stacks were taken using a *z*-axis stage controller at 0.2 mm intervals. For deconvolution, images were run through MicroTome deconvolution software. In some cases, the levels adjust function in Adobe Photoshop was used to spread the data-containing regions of the image across the full range of tonalities. When specifically indicated in the figure legends, specific images were enlarged, contrast enhanced, and/or inverted within Photoshop to visualize small structures better.

For DIC/Hoechst preparations, males were dissected in buffer with 100 µg/ml Hoechst 33342 (Sigma-Aldrich) on non-plus slides and immediately imaged.

Western blot

For western blot analysis, 100 worms were collected in 15-25 µl of M9 buffer in the cap of a 1.5 µl Eppendorf tube. Tubes were centrifuged for 1 min at 15,000 ***g***, immediately frozen in liquid nitrogen and stored at −80°C. Worm lysates from one freeze-thaw cycle were homogenized with a 4:100 mix of β-mercaptoethanol (MP Biomedicals) and sample buffer (NuPAGE LDS 4× Sample Buffer, Invitrogen) heated to 100°C, boiled for 5 min, and centrifuged for 8 min at 15,000 ***g***. Lysates from 50-100 worms were loaded per lane, and proteins were resolved at 150 V via SDS-PAGE (NuPAGE Novex 4-12% Bis-Tris, Invitrogen), and transferred to a PDVF

membrane (GE Healthcare). After blocking overnight with pH 8.0 Tris-buffered saline with 0.1% Tween20 containing either 4% non-fat dry milk (Carnation) or 5% bovine serum albumin (Sigma-Aldrich), membranes were incubated with the appropriate primary antibody diluted in blocking buffer (4% milk or 5% BSA in 1× TBST) for 2 h at room temperature, followed by incubation with 1:20,000 peroxidase-conjugated secondary antibody (Abcam) for 2 h at room temperature, and then developed by enhanced chemiluminescence (Immobilon Western Chemiluminescent HRP substrate, Millipore). SPE-18 protein was detected by a 1:5000 dilution of rabbit anti-SPE-18 polyclonal antibody (YenZym) and HRP-conjugated goat-anti rabbit IgG (Abcam, ab6721). MSP was detected by a 1:10,000 dilution of mouse anti-MSP monoclonal antibody 4A5 (Kosinski et al., 2005) and HRP-conjugated goat anti-mouse IgG (Abcam, ab6789).

Acknowledgements
Some strains were provided by the *Caenorhabditis* Genetics Center, which is funded by the NIH Office of Research Infrastructure Program [P40 OD010440]. We thank David Greenstein and Stephen L'Hernault for antibodies, and Harold Smith for the SPE-18-expressing *E. coli* strain. Lidia Epp (W&M molecular core technician) and undergraduates Alana Noritake and Bryan Neva assisted with the genetic and molecular identification of SPE-18 as F32A11.3. We thank Jordan Ward, Penny Sadler and Kayleigh Morrison for critical reading of this manuscript.

Competing interests
The authors declare no competing or financial interests.

Author contributions
Conceptualization: D.C.S.; Methodology: K.L.P., M.P., C.M.U., D.C.S.; Validation: K.L.P., M.P., C.M.U., D.C.S.; Formal analysis: K.L.P., M.P., C.M.U., D.C.S.; Investigation: K.L.P., M.P., C.M.U., D.C.S.; Writing - original draft: K.L.P., M.P., D.C.S.; Writing - review & editing: K.L.P., M.P., D.C.S.; Visualization: K.L.P., D.C.S.; Supervision: D.C.S.; Project administration: D.C.S.; Funding acquisition: D.C.S.

Funding
This work was supported by the National Institutes of Health [R15GM-096309 to D.C.S.] and the McLeod Tyler Professorship to D.C.S. Deposited in PMC for release after 12 months.

Supplementary information
Supplementary information available online at
https://dev.biologists.org/lookup/doi/10.1242/dev.195875.supplemental

Peer review history
The peer review history is available online at
https://dev.biologists.org/lookup/doi/10.1242/dev.195875.reviewer-comments.pdf

References
Blom, N., Gammeltoft, S. and Brunak, S. (1999). Sequence and structure-based prediction of eukaryotic protein phosphorylation sites. *J. Mol. Biol.* **294**, 1351-1362. doi:10.1006/jmbi.1999.3310

Bodakuntla, S., Jijumon, A. S., Villablanca, C., Gonzalez-Billault, C. and Janke, C. (2019). Microtubule-associated proteins: structuring the cytoskeleton. *Trends Cell Biol.* **29**, 804-819. doi:10.1016/j.tcb.2019.07.004

Brenner, S. (1974). The genetics of *Caenorhabditis elegans*. *Genetics* **77**, 71-94. doi:10.1093/genetics/77.1.71

Brouhard, G. J. and Rice, L. M. (2018). Microtubule dynamics: an interplay of biochemistry and mechanics. *Nat. Rev. Mol. Cell Biol.* **19**, 451-463. doi:10.1038/s41580-018-0009-y

Bullock, T. L., McCoy, A. J., Kent, H. M., Roberts, T. M. and Stewart, M. (1998). Structural basis for amoeboid motility in nematode sperm. *Nat. Struct. Biol.* **5**, 184-189. doi:10.1038/nsb0398-184

Buracco, S., Claydon, S. and Insall, R. (2019). Control of actin dynamics during cell motility. *F1000Res* **8**, 1977. doi:10.12688/f1000research.18669.1

Creamer, T. P. (2013). Transient disorder: calcineurin as an example. *Intrinsically Disord. Proteins* **1**, e26412. doi:10.4161/idp.26412

Chu, D. S. and Shakes, D. C. (2013). Spermatogenesis. *Adv. Exp. Med. Biol.* **757**, 171-203. doi:10.1007/978-1-4614-4015-4_7

Church, D. L., Guan, K. L. and Lambie, E. J. (1995). Three genes of the MAP kinase cascade, *mek*-2, *mpk*-1/*sur*-1 and *let*-60 ras, are required for meiotic cell cycle progression in *Caenorhabditis elegans*. *Development* **121**, 2525-2535.

de Forges, H., Bouissou, A. and Perez, F. (2012). Interplay between microtubule dynamics and intracellular organization. *Int. J. Biochem. Cell Biol.* **44**, 266-274. doi:10.1016/j.biocel.2011.11.009

Dyson, H. J. and Wright, P. E. (2002). Coupling of folding and binding for unstructured proteins. *Curr. Opin. Struct. Biol.* **12**, 54-60. doi:10.1016/S0959-440X(02)00289-0

Flock, T., Weatheritt, R. J., Latysheva, N. S. and Babu, M. M. (2014). Controlling entropy to tune the functions of intrinsically disordered regions. *Curr. Opin. Struct. Biol.* **26**, 62-72. doi:10.1016/j.sbi.2014.05.007

Gleason, E. J., Lindsey, W. C., Kroft, T. L., Singson, A. W. and L'Hernault, S. W. (2006). *spe-10* encodes a DHHC-CRD zinc-finger membrane protein required for endoplasmic reticulum/Golgi membrane morphogenesis during *Caenorhabditis elegans* spermatogenesis. *Genetics* **172**, 145-158. doi:10.1534/genetics.105.047340

Goodson, H. V. and Jonasson, E. M. (2018). Microtubules and microtubule-associated proteins. *Cold Spring Harb. Perspect. Biol.* **10**, a022608. doi:10.1101/cshperspect.a022608

Hernández-Vega, A., Braun, M., Scharrel, L., Jahnel, M., Wegmann, S., Hyman, B. T., Alberti, S., Diez, S. and Hyman, A. A. (2017). Local nucleation of microtubule bundles through tubulin concentration into a condensed Tau phase. *Cell Rep.* **20**, 2304-2312. doi:10.1016/j.celrep.2017.08.042

Hohmann, T. and Dehghani, F. (2019). The cytoskeleton-A complex interacting meshwork. *Cells* **8**, 362. doi:10.3390/cells8040362

Hu, J., Cheng, S., Wang, H., Li, X., Liu, S., Wu, M., Liu, Y. and Wang, X. (2019). Distinct roles of two myosins in *C. elegans* spermatid differentiation. *PLoS Biol.* **17**, e3000211. doi:10.1371/journal.pbio.3000211

Ishida, T. and Kinoshita, K. (2007). PrDOS: prediction of disordered protein regions from amino acid sequence. *Nucleic Acids Res.* **35**, W460-W464. doi:10.1093/nar/gkm363

Italiano, J. E., Jr, Roberts, T. M., Stewart, M. and Fontana, C. A. (1996). Reconstitution *in vitro* of the motile apparatus from the amoeboid sperm of Ascaris shows that filament assembly and bundling move membranes. *Cell* **84**, 105-114. doi:10.1016/S0092-8674(00)80997-6

Italiano, J. E., Jr, Stewart, M. and Roberts, T. M. (1999). Localized depolymerization of the major sperm protein cytoskeleton correlates with the forward movement of the cell body in the amoeboid movement of nematode sperm. *J. Cell Biol.* **146**, 1087-1096. doi:10.1083/jcb.146.5.1087

Jaramillo-Lambert, A., Ellefson, M., Villeneuve, A. M. and Engebrecht, J. (2007). Differential timing of S phases, X chromosome replication, and meiotic prophase in the *C. elegans* germ line. *Dev. Biol.* **308**, 206-221. doi:10.1016/j.ydbio.2007.05.019

Jiang, H., Wang, S., Huang, Y., He, X., Cui, H., Zhu, X. and Zheng, Y. (2015). Phase transition of spindle-associated protein regulate spindle apparatus assembly. *Cell* **163**, 108-122. doi:10.1016/j.cell.2015.08.010

Kelley, L. A., Mezulis, S., Yates, C. M., Wass, M. N. and Sternberg, M. J. E. (2015). The Phyre2 web portal for protein modeling, prediction and analysis. *Nat. Protoc.* **10**, 845-858. doi:10.1038/nprot.2015.053

Kim, A. S., Kakalis, L. T., Abdul-Manan, N., Liu, G. A. and Rosen, M. K. (2000). Autoinhibition and activation mechanisms of the Wiskott–Aldrich syndrome protein. *Nature* **404**, 151-158. doi:10.1038/35004513

King, M. R. and Petry, S. (2020). Phase separation of TPX2 enhances and spatially coordinates microtubule nucleation. *Nat. Commun.* **11**, 270. doi:10.1038/s41467-019-14087-0

King, K. L., Stewart, M., Roberts, T. M. and Seavy, M. (1992). Structure and macromolecular assembly of two isoforms of the major sperm protein (MSP) from the amoeboid sperm of the nematode, *Ascaris suum*. *J. Cell Sci.* **101**, 847-857. doi:10.1006/jmbi.1993.1383

King, K. L., Essig, J., Roberts, T. M. and Moerland, T. S. (1994a). Regulation of the Ascaris major sperm protein (MSP) cytoskeleton by intracellular pH. *Cell Motil. Cytoskeleton* **27**, 193-205. doi:10.1002/cm.970270302

King, K. L., Stewart, M. and Roberts, T. M. (1994b). Supramolecular assemblies of the *Ascaris suum* major sperm protein (MSP) associated with amoeboid cell motility. *J. Cell Sci.* **107**, 2941-2949.

Klass, M. R. and Hirsh, D. (1981). Sperm isolation and biochemical analysis of the major sperm protein from *Caenorhabditis elegans*. *Dev. Biol.* **84**, 299-312. doi:10.1016/0012-1606(81)90398-5

Kosinski, M., McDonald, K., Schwartz, J., Yamamoto, I. and Greenstein D. (2005). *C. elegans* sperm bud vesicles to deliver a meiotic maturation signal to distant oocytes. *Development* **132**, 3357-3369. doi:10.1242/dev.01916

Kulkarni, M., Shakes, D. C., Guevel, K. and Smith, H. E. (2012). SPE-44 implements sperm cell fate. *PLoS Genet.* **8**, e1002678. doi:10.1371/journal.pgen.1002678

LeClaire, L. L., III, Stewart, M. and Roberts, T. M. (2003). A 48 kDa integral membrane phosphoprotein orchestrates the cytoskeletal dynamics that generate amoeboid cell motility in Ascaris sperm. *J. Cell Sci.* **116**, 2655-2663. doi:10.1242/jcs.00469

L'Hernault, S. W., Shakes, D. C. and Ward, S. (1988). Developmental genetics of chromosome I spermatogenesis-defective mutants in the nematode *Caenorhabditis elegans*. *Genetics* **120**, 435-452. doi:10.1093/genetics/120.2.435

Madeira, F., Park, Y. M., Lee, J., Buso, N., Gur, T., Madhusoodanan, N., Basutkar, P., Tivey, A. R. N., Potter, S. C., Finn, R. D. et al. (2019). The EMBL-EBI search and sequence analysis tools APIs in 2019. *Nucleic Acids Res.* **47**, W636-W641. doi:10.1093/nar/gkz268

Miller, D. M. and Shakes, D. C. (1995). Immunofluorescence microscopy. *Methods Cell Biol.* **48**, 365-394. doi:10.1016/S0091-679X(08)61396-5
Miller, M. A., Nguyen, V. Q., Lee, M. H., Kosinski, M., Schedl, T., Caprioli, R. M. and Greenstein, D. (2001). A sperm cytoskeletal protein that signals oocyte meiotic maturation and ovulation. *Science* **16**, 2144-2147. doi:10.1126/science.1057586
Montenegro Gouveia, S., Zitouni, S., Kong, D., Duarte, P., Ferreira Gomes, B., Sousa, A. L., Tranfield, E. M., Hyman, A., Loncarek, J. and Bettencourt-Dias, M. (2018). PLK4 is a microtubule-associated protein that self-assembles promoting *de novo* MTOC formation. *J. Cell Sci.* **132**, jcs219501. doi:10.1242/jcs.219501
Muhlrad, P. J. and Ward, S. (2002). Spermiogenesis initiation in *Caenorhabditis elegans* involves a casein kinase 1 encoded by the *spe*-6 gene. *Genetics* **161**, 143-155.
Nelson, G. A., Roberts, T. M. and Ward, S. (1982). *Caenorhabditis elegans* spermatozoan locomotion: amoeboid movement with almost no actin. *J. Cell Biol.* **92**, 121-131. doi:10.1083/jcb.92.1.121
Nishimura, H. and L'Hernault, S. W. (2010). Spermatogenesis-defective (spe) mutants of the nematode *Caenorhabditis elegans* provide clues to solve the puzzle of male germline functions during reproduction. *Dev. Dyn.* **239**, 1502-1514. doi:10.1002/dvdy.22271
Okamoto, H. and Thomson, J. N. (1985). Monoclonal antibodies which distinguish certain classes of neuronal and supporting cells in the nervous tissue of the nematode *Caenorhabditis elegans*. *J. Neurosci.* **5**, 643-653. doi:10.1523/JNEUROSCI.05-03-00643.1985
Pancsa, R. and Fuxreiter, M. (2012). Interactions via intrinsically disordered regions: what kind of motifs? *IUBMB Life* **64**, 513-520. doi:10.1002/iub.1034
Radivojac, P., Vacic, V., Haynes, C., Cocklin, R. R., Mohan, A., Heyen, J. W., Goebl, M. G. and Iakoucheva, L. M. (2010). Identification, analysis, and prediction of protein ubiquitination sites. *Proteins* **78**, 365-380. doi:10.1002/prot.22555
Ragle, J. M., Aita, A. L., Morrison, K. N., Martinez-Mendez, R., Saeger, H. N., Ashley, G. A., Johnson, L. C., Schubert, K. A., Shakes, D. C. and Ward, J. D. (2020). The conserved molting/circadian rhythm regulator NHR-23/NR1F1 serves as an essential co-regulator of *C. elegans* spermatogenesis. *Development* **147**, dev193862. doi:10.1242/dev.193862
Reinke, V., Smith, H. E., Nance, J., Wang, J., Van Doren, C., Begley, R., Jones, S. J. M., Davis, E. B., Scherer, S., Ward, S. et al. (2000). A global profile of germline gene expression in *C. elegans*. *Mol. Cell* **6**, 605-616. doi:10.1016/S1097-2765(00)00059-9
Reinke, V., Gil, I. S., Ward, S. and Kazmer, K. (2004). Genome-wide germline-enriched and sex-biased expression profiles in *Caenorhabditis elegans*. *Development* **131**, 311-323. doi:10.1242/dev.00914
Roberts, T. M. (2005). Major sperm protein. *Curr. Biol.* **15**, R153. doi:10.1016/j.cub.2005.02.036
Roberts, T. M. and Stewart, M. (2012). Role of major sperm protein (MSP) in the protrusion and retraction of Ascaris sperm. *Int. Rev. Cell Mol. Biol.* **297**, 265-293. doi:10.1016/B978-0-12-394308-8.00007-8
Roberts, T. M., Pavalko, F. M. and Ward, S. (1986). Membrane and cytoplasmic proteins are transported in the same organelle complex during nematode spermatogenesis. *J. Cell Biol.* **102**, 1787-1796. doi:10.1083/jcb.102.5.1787
Rottner, K., Faix, J., Bogdan, S., Linder, S. and Kerkhoff, E. (2017). Actin assembly mechanisms at a glance. *J. Cell Sci.* **130**, 3427-3435. doi:10.1242/jcs.206433
Roy, A., Kucukural, A. and Zhang, Y. (2010). I-TASSER: a unified platform for automated protein structure and function prediction. *Nat. Protoc.* **5**, 725-738. doi:10.1038/nprot.2010.5
Sepsenwol, S., Ris, H. and Roberts, T. M. (1989). A unique cytoskeleton associated with crawling in the amoeboid sperm of the nematode, *Ascaris suum*. *J. Cell Biol.* **108**, 55-66. doi:10.1083/jcb.108.1.55
Shakes, D. C. and Ward, S. (1989). Mutations that disrupt the morphogenesis and localization of a sperm-specific organelle in *Caenorhabditis elegans*. *Dev. Biol.* **134**, 307-316. doi:10.1016/0012-1606(89)90103-6
Shakes, D. C., Wu, J.-C., Sadler, P. L., Laprade, K., Moore, L. L., Noritake, A. and Chu, D. S. (2009). Spermatogenesis-specific features of the meiotic program in *Caenorhabditis elegans*. *PLoS Genet.* **5**, e1000611. doi:10.1371/journal.pgen.1000611
Sharma, R., Raduly, Z., Miskei, M. and Fuxreiter, M. (2015). Fuzzy complexes: specific binding without complete folding. *FEBS Lett.* **589**, 2533-2542. doi:10.1016/j.febslet.2015.07.022
Shin, Y. and Brangwynne, C. P. (2017). Liquid phase condensation in cell physiology and disease. *Science* **357**, eaaf4382. doi:10.1126/science.aaf4382
Singson, A. (2001). Every sperm is sacred: fertilization in *Caenorhabditis elegans*. *Dev. Biol.* **230**, 101-109. doi:10.1006/dbio.2000.0118
Smith, H. E. (2014). Nematode sperm motility. WormBook, ed. The C. elegans Research Community. doi:10.1895/wormbook.1.68.2, http://www.wormbook.org
Sulston, J. and Hodgkin, J. (1988). Methods. In *The Nematode Caenorhabditis elegans* (ed. W. B. Wood), pp. 587-606. Cold Spring Harbor: Cold Spring Harbor Laboratory Press.
Svitkina, T. M. (2018). Ultrastructure of the actin cytoskeleton. *Curr. Opin. Cell Biol.* **54**, 1-8. doi:10.1016/j.ceb.2018.02.007
Swan, K. A., Curtis, D. E., McKusick, K. B., Voinov, A. V., Mapa, F. A. and Cancilla, M. R. (2002). High-throughput gene mapping in *Caenorhabditis elegans*. *Genome Res.* **12**, 1100-1105.
Uversky, V. N. (2017). Paradoxes and wonders of intrinsic disorder: stability of instability. *Intrinsically Disord. Proteins* **5**, e1327757. doi:10.1080/21690707.2017.1327757
Varkey, J. P., Jansma, P. L., Minniti, A. N. and Ward, S. (1993). The *Caenorhabditis elegans spe*-6 gene is required for major sperm protein assembly and shows second site non-complementation with an unlinked deficiency. *Genetics* **133**, 79-86. doi:10.1093/genetics/133.1.79
Ward, S. (1986). The asymmetric localization of gene products during the development of *Caenorhabditis elegans* spermatozoa. In *Gametogenesis and the Early Embryo* (ed. J. Gall), pp. 55-75. New York: A.R. Liss.
Ward, S., Argon, Y. and Nelson, G. A. (1981). Sperm morphogenesis in wild-type and fertilization-defective mutants of *Caenorhabditis elegans*. *J. Cell Biol.* **91**, 26-44. doi:10.1083/jcb.91.1.26
Weirich, K. L., Banerjee, S., Dasbiswas, K., Witten, T. A., Vaikuntanathan, S. and Gardel, M. L. (2017). Liquid behavior of cross-linked actin bundles. *Proc. Natl. Acad. Sci. USA* **114**, 2131-2136. doi:10.1073/pnas.1616133114
Winter, E. S., Schwarz, A., Fabig, G., Feldman, J. L., Pires-daSilva, A., Müller-Reichert, T., Sadler, P. L. and Shakes, D. C. (2017). Cytoskeletal variations in an asymmetric cell division support diversity in nematode sperm size and sex ratios. *Development* **144**, 3253-3263. doi:10.1242/dev.153841
Wu, J.-C., Go, A. C., Samson, M., Cintra, T., Mirsoian, S., Wu, T. F., Jow, M. M., Routman, E. J. and Chu, D. S. (2012). Sperm development and motility are regulated by PP1 phosphatases in *Caenorhabditis elegans*. *Genetics* **190**, 143-157. doi:10.1534/genetics.111.135376
Yan, R., Xu, D., Yang, J., Walker, S. and Zhang, Y. (2013). A comparative assessment and analysis of 20 representative sequence alignment methods for protein structure prediction. *Sci. Rep.* **3**, 2619. doi:10.1038/srep02619
Yi, K., Wang, X., Emmett, M. R., Marshall, A. G., Stewart, M. and Roberts, T. M. (2009). Dephosphorylation of major sperm protein (MSP) fiber protein 3 by protein phosphatase 2A during cell body retraction in the MSP-based amoeboid motility of Ascaris sperm. *Mol. Biol. Cell* **20**, 3200-3208. doi:10.1091/mbc.e09-03-0240

SUPPLEMENTARY MATERIAL

Table S1. *spe-18* genetic mapping data

Two-factor mapping

Genotype	**Recombinants**	**Segregation**
unc-4 spe-18 / + +	Unc Non-Spe	8/72
rol-1 spe-18 / + +	Rol Non-Spe	13/114

SNIP SNP mapping (Rol Non-Spe recombinants)

Marker	**Genetic**	**Molecular**	**Marker N2**
unc-4	1.77	9898 kb	
rol-1	6.90	12172 kb	
pkP2112	13.20	12990 kb	5/18
pkP2116	16.09	13235 kb	0/18
pkP2154	19.17	13647 kb	1*/17

*presumed double-cross over event

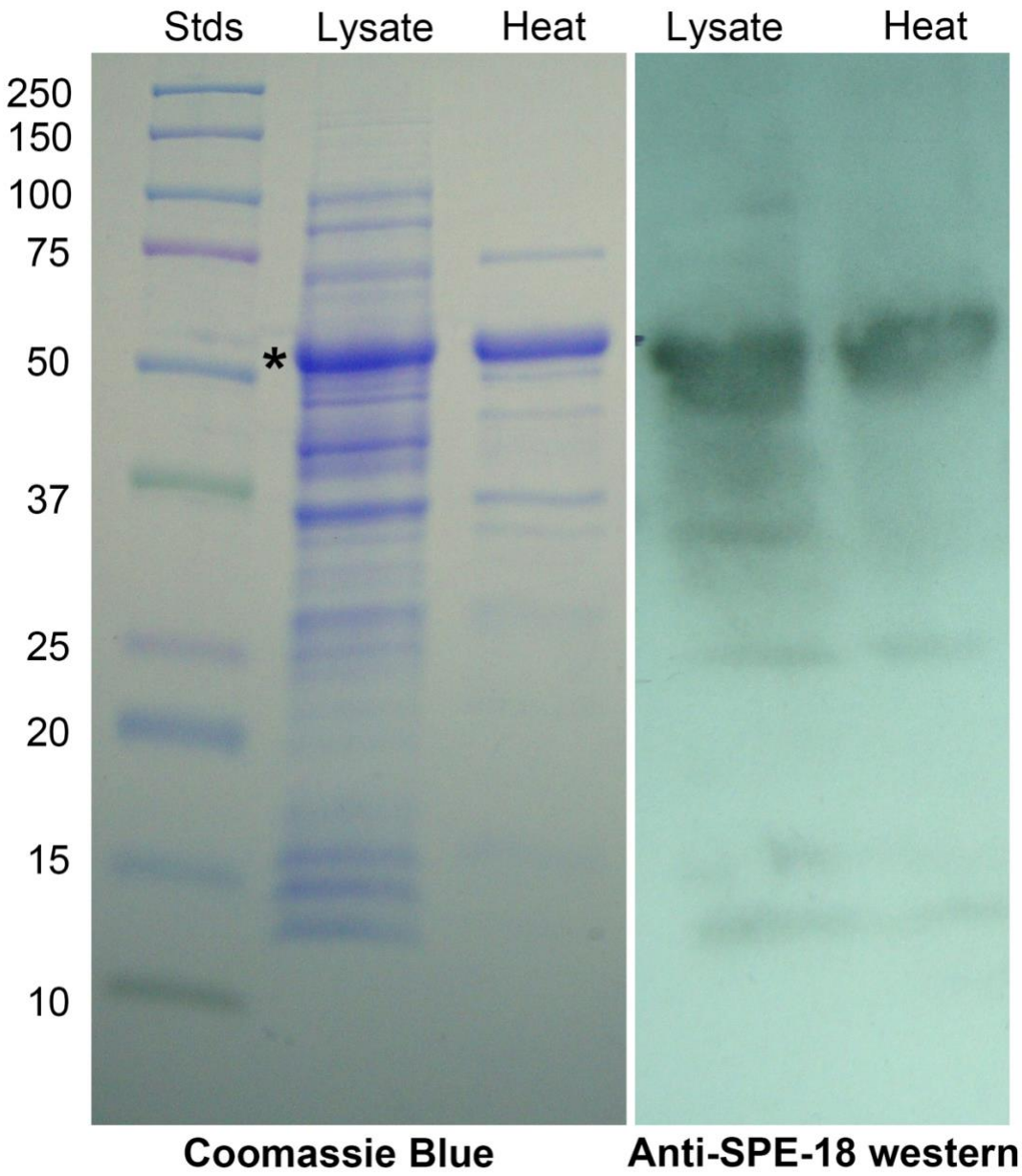

Figure S1. Heat treatment of supernatant +/- 95^{o}C heat treatment from *E. coli* expression *C. elegans* SPE-18 fused to an 8.2 kDa Profinity eXact tag (Bio-Rad). The Coomassie blue gel of lysate from induced bacteria and corresponding western blot with anti-SPE-18 antibody (see methods and figure 4 for antibody details).

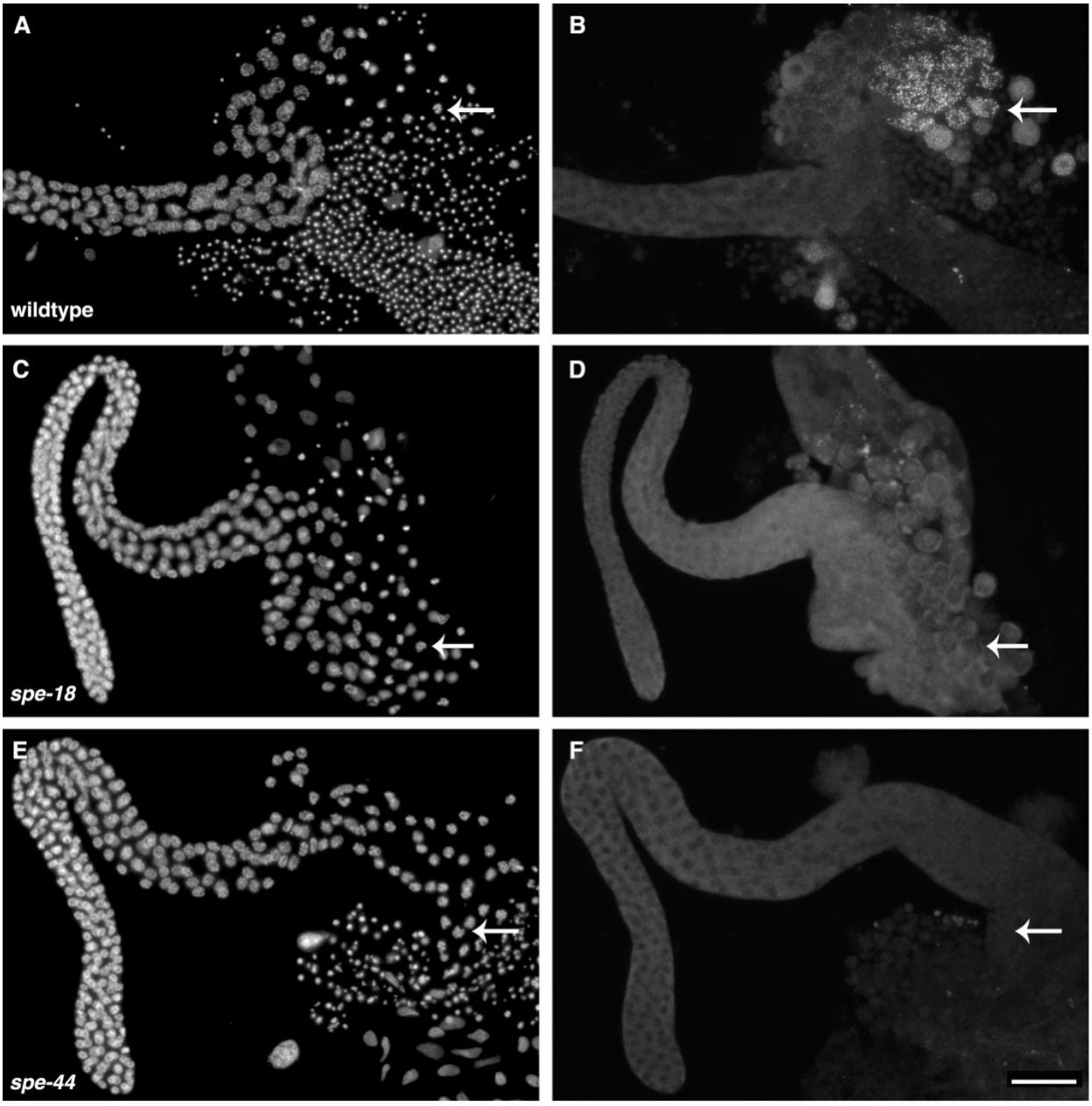

Figure S2. Isolated whole gonads from wildtype, *spe-18*, and *spe-44* males co-labelled with DAPI (A,C,E) and anti-SPE-18 antibodies (B,D,F). Arrows indicated metaphase I spermatocytes. Samples were prepared at the same time and photographed with identical exposures. Scale bar = 20 microns.

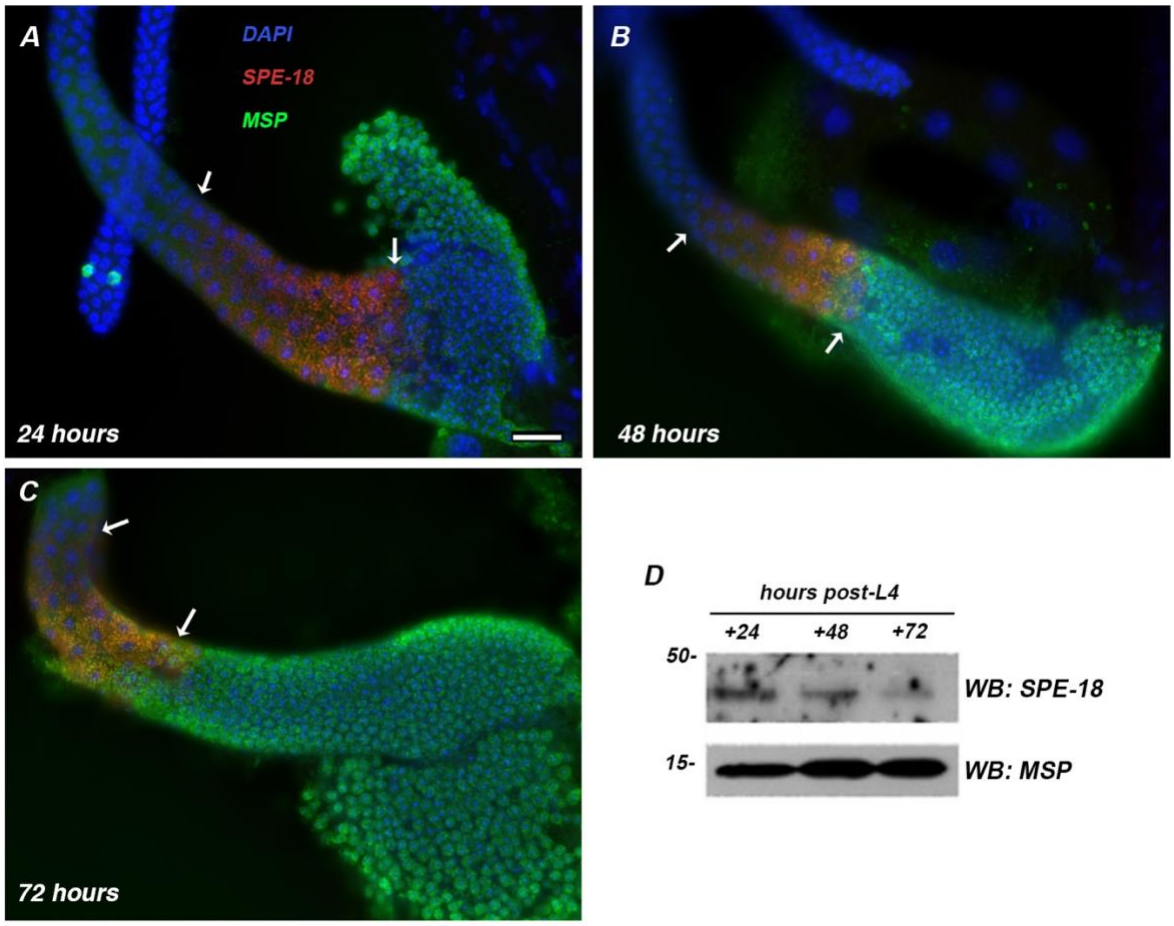

Figure S3. Isolated gonads co-labelled with DAPI(blue), anti-SPE-18 (red), and anti-MSP(green) antibody in synchronized, aging celibate wildtype males (A-C) and anti-SPE-18 western blot of sibling male populations (D). Arrows delineate the boundaries of SPE-18 labelling within each gonad. Scale bar = 10 microns.